CALIFORNIA COASTAL COMMISSION
455 MARKET STREET, SUITE 300
SAN FRANCISCO, CA 94105-2219
FAX (415) 904-5400
TDD (415) 597-5885

Th12a

ADDENDUM

October 11, 2022

TO: Coastal Commissioners and Interested Parties

FROM: Kate Huckelbridge, Senior Deputy Director
Cassidy Teufel, Manager, Energy Ocean Resources, and Federal Consistency Division
Holly Wyer, Senior Environmental Scientist, Energy, Ocean Resources, and Federal Consistency Division

SUBJECT: **ADDENDUM TO AGENDA ITEM TH12A, APPLICATION NO E-00-014-A2 (SOUTHERN CALIFORNIA EDISON), THURSDAY, OCTOBER 13, 2022**

The purpose of this addendum is to resolve minor inaccuracies and respond to public comments received since publication of the staff report. The correspondence received is included under the correspondence tab for this item on the Commission's website. This addendum hereby incorporates into the staff recommendation for agenda item Th12a (CDP Application No. E-00-014-A2) and into the pertinent Coastal Commission findings otherwise set forth in the September 23, 2022, staff report, the following changes. In responding to comments received, Commission staff also hereby revises the staff report and, thereby, its proposed Commission findings, consistent with the responses provided herein.

I. CHANGES TO THE STAFF REPORT

The following are revisions to the text of the staff report and recommendation. Language changes were made to enhance clarity of the conditions and findings. Proposed deletions are marked with ~~strikethrough~~ text and additions are marked with <u>underlined</u> text.

a) Addition of text in the summary of staff recommendation on page 1:

Southern California Edison (SCE), on behalf of itself and the other <u>current and former</u> co-owners of the San Onofre Nuclear Generating Station (SONGS), <u>including</u> San

Diego Gas and Electric, the City of Anaheim, and the City of Riverside, requests an amendment to Coastal Development Permit (CDP) No. E-00-014 to extend the authorization term of the Nuclear Horizontal Modular Storage (NUHOMS) nuclear waste storage facility[1] at the SONGS site to November 15, 2035.

b) Addition of text in footnote 3 on page 12:

SCE has submitted the amendment application and is acting as the applicant on behalf of itself and all the co-owners of SONGS. In addition to SCE, the current and former owners ~~include~~ are: San Diego Gas and Electric, the City of Anaheim, and the City of Riverside.

c) Changes to text and numbering in Condition 6 on page 8:

6. **Aging Management Program Review and Reporting of Inspection Results.**
    a. By January 1, 2024, the permittee shall fund an independent, third-party review of the following in permittee's existing AMP and Implementing Procedures (AMP) for the NUHOMS ISFSI: (1) The canister inspection, monitoring and maintenance techniques that will be implemented, including prospective non-destructive examination techniques and remote surface inspection tools; (2) what data will be collected and reporting frequency; (3) all available evidence related to the physical condition of the canisters and their susceptibility to degradation processes such as stress corrosion cracking, including any available, pre-existing inspection documentation, photographs, and videos (such as those collected in November 2021 by Orano as it performed the NRC-required AMP inspection for the SONGS NUHOMS ISFSI); and (4) remediation measures that will be implemented, including the submission of a coastal development permit amendment application, if the results of the canister inspection and maintenance do not ensure that the fuel storage canisters will remain in a physical condition sufficient to allow on-site transfer and offsite transport for the term of the project as authorized under Special Condition 4.
        i. ….
    ~~c.~~ d. The findings of the independent, third-party review shall be reported in writing to the Executive Director by July 1, 2024…
    ~~d.~~ e. As part of the AMP, the permittee shall perform required inspections of the ISFSI and spent fuel canisters no less frequently than once every five years…

d) Revision and addition of text in the waste storage facility details section on pages 13-14:

In total, the NUHOMS waste storage facility has a capacity under its current build-out for 63 steel reinforced spent fuel storage modules on top of ~~three~~ two steel-reinforced concrete pads.

[1] The technical term for the waste storage facility is an Independent Spent Fuel Storage Installation (ISFSI). Prior staff reports for this facility used this term and this acronym appears in the recommended special conditions and may also appear in some quotes within these findings.

The concrete pads are reinforced with rebar and are a minimum of three feet thick, with the top being at existing grade elevation, approximately 20 ft mean lower low water (MLLW)[2], and are approximately 43 ft and 60 ft wide, respectively. …

Each spent fuel storage module houses an NRC-licensed stainless steel canister that ~~may~~ contains either greater-than-class-C material or spent fuel assemblies. For example, a typical Unit 2/3 canister contains up to 24 spent fuel assemblies. A Unit 2/3 fuel assembly consists of 236 zircalloy metal tubes approximately 12.8 ft long and 3/8 inch in diameter, in which ceramic uranium dioxide fuel pellets are placed.

e) Revision and addition of text in the Other Agency Approvals and Coordination section, specifically the United States Department of the Navy section on page 17:

SCE operates the SONGS site under the terms of a grant of easement from the U.S. Department of the Navy (Navy). The grant of easement was executed on May 12, 1964, and is effective through May 12, 2024. ~~SCE is in the process of applying for an extension of the grant of easement from the Navy~~ has submitted an application to the Navy to extend the current easement.

f) Revision and addition of text in the ground shaking analysis on page 21:

In recent months, new research has emerged indicating that the Palos Verdes Fault Zone, another largely offshore fault system (extending from Santa Monica Bay, across the Palos Verdes Peninsula, to the area offshore northern San Diego County) occurring farther west than the Newport Inglewood Rose Canyon Fault System (NIRC), may be capable of producing larger earthquakes than previously thought (Wolfe et al. 2022). The new study presents a revised model of the Palos Verdes Fault Zone and postulates that a multi-segment rupture on this system could produce earthquakes with magnitudes in the range of M 7.4 – 7.8. Previous seismic hazards assessments for the SONGS site (e.g., GeoPentch 2010, Coastal Environment 2022a) considered the potential hazard from an approximately M 7.0 earthquake on the Palos Verdes fault system, finding that the expected ground shaking at SONGS was much less than that associated with an event on the NIRC system, mostly due to the greater distance between the nearest Palos Verdes fault segment (approximately 17 miles) and the SONGS site. In order to address the new study, SCE has provided the results of a new ground shaking analysis of a M7.8 earthquake on the Palos Verdes Fault Zone, including the segment closest to SONGS (Coastal Environments 2022d). The estimated peak ground acceleration (PGA) for this event was 0.19 g, significantly lower than the PGA values estimated for the M 7.6 multi-segment earthquake scenario on the Coastal Fault System (including the NIRC), and less than 13 percent of the design PGA value (1.5 g) of the NUHOMS waste storage facility. This analysis indicates that large earthquakes on the much nearer NIRC system (and linked faults) remain the primary ground shaking hazard at the SONGS site, and that the design of the waste storage facility continues to minimize ground-shaking hazards.

Based on the available information, ~~The 1.5g peak ground acceleration established for~~ the waste storage facility design remains conservative for the seismic hazards identified for the SONGS site, even in light of the new ~~modeling~~ information ~~that accounts for recent earthquake information~~ related to the postulated extreme

[2] SCE uses MLLW from the 1941-1959 tidal datum epoch for consistent use across old engineering drawings; MLLW in this case can be converted to NAVD88 by subtracting 0.62 ft.

earthquake events on the Coastal Fault System and NIRC and Palos Verdes Fault Zone.

g) Revision of text in the far-field tsunamis section on page 24:

This would be below the top of the NUHOMS waste storage facility concrete module height of ~~32.5 ft~~ 40.3 ft MLLW, and much lower than the waste storage facility water submergence design depth of 50 ft.

h) Revision of text in the submarine landslide tsunamis section on page 26:

All of these inundation depths are below the concrete module height of ~~32.5 ft~~ 40.3 ft, and are much lower than the waste storage facility submergence design of 50 ft.

i) Revision and addition of text in the future on-site alternatives and managed retreat section on page 29:

~~The remainder of the SONGS facilities are~~ The Units 2 and 3 portion of the SONGS site is currently in the process of being decommissioned. Once the Units 2 and 3 decommissioning is complete in approximately 2028, the only above-grade structures aside from the NUHOMS and Holtec waste storage facilities that will remain on the site are the revetment, walkway, seawall, and electrical switchyard.

j) Addition of text to the environmental justice coastal act analysis on pages 34-35:

SCE also works closely with unions such as Laborers International Union of North America and Valentine ("Val") Macedo, LiUNA Local 89, Business Manager, to ensure that on-site workers at SONGS receive updates on decommissioning and other relevant activities.

k) Addition of text to the visual resources section on page 35:

Once the decommissioning process for Units 2 and 3 is complete in approximately 2028, the only above-grade structures aside from the two dry storage facilities that will remain on the site are the revetment, walkway, seawall, and electrical switchyard.

II. CHANGES TO APPENDIX A

The following are text changes to Appendix A and additional attachments to Appendix A are included with this Addendum.

i. Addition of the following citations:

Coastal Environments, Inc. (2022d). Geological and Tsunami Hazards/Palos Verdes Fault Zone. Attached

Wolfe, F., Shaw, J., Plesch, A. (2022). *Origin of the Palos Verde Restraining Bend and its Implications for the 3D Geometry of the Fault and Earthquake Hazards in Los Angeles, California*. Bulletin of the Seismological Society of America. Attached.

III. CORRESPONDENCE RECEIVED AND STAFF RESPONSE

The Commission received correspondence from commenters, some of which requested modifications to the text of the staff report. The main points of these requests and the responses to them are as follows:

1. Request: Several commenters requested additional findings and conditions relating to nuclear safety, these include repacking the canisters with fewer spent fuel assemblies to lower their weight, ensure that canisters would not crack if they fell off a train/truck while being transported, and assessing the consequences of accidents at the NUHOMS waste storage facility.

   Response: These concerns and requests relate to nuclear safety or radiological issues. As discussed in the staff report, the Nuclear Regulatory Commission has exclusive jurisdiction over all radiological elements and safety of SONGS and the NUHOMS waste storage facility. The staff report only addresses state concerns related to the project's conformity to applicable policies of the Coastal Act.

2. Request: A commenter noted that the recent earthquake estimates are based on a maximum 7.5 magnitude earthquake, but that experts now believe that the Palos Verdes Fault is capable of producing a 7.8 magnitude (M) earthquake.

   Response: The study identifying the possibility for a larger earthquake on the Palos Verdes Fault was reviewed by the Commission's staff geologist and SCE. In addition, SCE prepared and provided with its comment letter on this item (included in the correspondence packet available on the Commission's online agenda) a new analysis of ground shaking from a M 7.8 earthquake on the Palos Verdes Fault Zone. This review and analysis found that peak ground acceleration (PGA) at SONGS from an M7.8 earthquake on the Palos Verdes Fault Zone would be 0.19 g, significantly lower than the PGA values estimated for the M 7.6 multi-segment earthquake scenario on the closer Coastal Fault System (including the NIRC), and less than 13 percent of the design PGA value (1.5 g) of the NUHOMS waste storage facility. Please refer to the text changes noted above in Section I(f) for more detail.

3. Request: A commenter requested a third-party detailed review of the inspection process and inspection videos of the oldest canister in the NUHOMS waste storage facility.

   Response: The Aging Management Program inspections in 2021 were performed by a third-party contractor, Orano, using a robot. Public information on the inspections and results is available on the SONGS Community Website, and includes a link to the Inspection Summary[3]. The specific request for a third-party review of the Aging Management Program and Implementation Procedures is addressed in the staff report through Condition 6, which requires an independent review of the Aging Management Program. Language has been added to Condition 6 to clarify that the independent review would also include review of existing inspection documentation, including all available videos and photographs. Please refer to the text changes noted above in above in Section I(c) for more detail.

[3] https://s3.amazonaws.com/cms.ipressroom.com/339/files/20224/Orano+AMP+Inspection+Summary+2022.pdf

Attachments for Appendix A

CE **Coastal Environments, Inc.**
Oceanographic and Coastal Services

6 October 2022

Ronald Pontes
Southern California Edison
2244 Walnut Grove Avenue
Rosemead, CA 91770

Subject: Geological and Tsunami Hazards / Palos Verdes Fault Zone

Dear Mr. Pontes,

Below is our response to your question regarding seismic and tsunami hazards considering the recent paper regarding the Palos Verdes fault zone.

Question:

In light of the recent paper by Wolfe et al. (2022) entitled "Origin of the Palos Verdes Restraining Bend and Its Implications for the 3 D Geometry of the Fault and Earthquake Hazards in Los Angeles, California" (Wolfe Paper) about the Palos Verdes fault zone, do the seismic and tsunami analyses prepared for the NUHOMS ISFSI CDP remain valid?

Answer:

The Wolfe Paper does not alter the conclusions in the seismic and tsunami reports submitted in support of the NUHOMS CDP Amendment Application. The postulated seismic and tsunami hazards from the Palos Verdes fault zone would not exceed those identified in the seismic and tsunami reports.

1. Seismic Hazards

The seismic hazards identified in the Wolfe Paper do not present a greater seismic hazard at SONGS than the greatest postulated seismic event discussed in the geological hazards report submitted in support of the NUHOMS CDP Amendment Application.

The Palos Verdes fault zone has been identified and mapped by numerous investigators for decades, including scientists at the US Geological Survey, California Geological Survey, and Southern California Earthquake Center. The Wolfe Paper presents a revised model of the Palos Verdes fault zone that emphasizes the complex mapped fault patterns that could combine to produce large earthquakes, Mw 7.4 - 7.8, during multi-segment ruptures.

The overall length of the revised model of the Palos Verdes fault zone is estimated to be 110 km, reaching from the Santa Monica fault near Point Dume in Santa Monica Bay to the northern end of the San Diego Trough. The maximum magnitude potential identified in the revised model requires rupture of all the combined fault segments and branches in an extreme earthquake.

Ground shaking hazard, measured by the horizontal Peak Ground Acceleration (PGA), is estimated using Ground Motion Prediction Equations such as the GK15 version that was used to estimate shaking hazards for SONGS. The estimated PGA at SONGS from a Mw7.8 earthquake along the Palos Verdes fault zone, including the Lasuen Knoll segment (which is the closest portion of the Palos Verdes fault zone, at 28 km from SONGS), would be **0.19g**. That value is less than 40 percent of the **0.51g** PGA estimated for the Mw7.6 earthquake scenario along the Coastal Fault System that includes Newport-Inglewood, Rose Canyon and linked faults from Newport Beach to La Jolla (Coastal Environments, 2022a). The Mw7.6 Coastal Fault System earthquake was the largest postulated earthquake modeled in the seismic report submitted in support of the NUHOMS ISFSI CDP Amendment Application.

2. Tsunami Hazards

Potential tsunamis from the revised model also would not present a greater tsunami hazard at SONGS than the greatest tsunami event discussed in the tsunami hazards report submitted in support of the NUHOMS ISFSI CDP Amendment Application.

Tsunami runup along a coastal site depends on 1) the seafloor displacement during the source (earthquake for this study), 2) the distance from the seafloor displacement to the site, 3) the configuration of the seafloor displacement (elongate, irregular with high-slip patches, etc.), and 4) seafloor morphology (bathymetry) that may focus or dissipate tsunami wave energy along the source-to-site propagation path.

In light of the Wolfe Paper, the following discussion compares tsunami hazards identified in the tsunami report submitted in support of the NUHOMS ISFSI CDP Amendment Application (i.e., from a) an Eastern Aleutian source, which is the largest tsunami overall, and b) the Coastal Fault System), against c) a postulated tsunami generated from revised model of the Palos Verdes fault zone. As described below, the largest postulated tsunami is from an Eastern Aleutian source, which was already considered in the tsunami report.

a. Eastern Aleutian Subduction Zone

The Eastern Aleutian subduction zone would produce the largest potential tsunami at SONGS. This is because of factors 1, 3 and 4 described above. For the Eastern Aleutian zone, the seafloor displacement would be very large. Fault displacement of 33.25 m, based on a maximum postulated earthquake of Mw9.5, would produce 4.5 - 5.0 m tsunami amplitude at the source. The configuration is broad (1500 km) and its east-west orientation focuses the wave energy southeast toward Southern California, and the seafloor morphology contributes to the severity of the tsunami as it approaches the Southern California coast. Although the distance from the Eastern Aleutian subduction zone to SONGS is more than two thousand miles (about 4000 km), much farther than the other two systems below, these three factors overcome the distance and make it the largest potential tsunami threat.

The Eastern Aleutians worst-case model (EA-sc3) would produce a maximum wave amplitude offshore SONGS of 7.77 m, with runup of 8.67 m NAVD88 at SONGS.

b. Coastal Fault System – Newport-Inglewood, Rose Canyon, San Mateo, San Onofre, Carlsbad fault Sections

The Coastal Fault System (Newport-Inglewood, Rose Canyon, San Mateo, San Onofre, Carlsbad fault sections) is the closest to SONGS of all tsunami sources, with Newport-Inglewood fault segment located about 7 km from SONGS.

The largest postulated earthquake of Mw7.62 for this system involves a 9-segment earthquake rupture that stretches about 92 km along the Southern California coast from Encinitas to Newport Beach. The model includes a 2-segment San Mateo Thrust source located about 15 km offshore. The modeled fault displacements of 4.0 m and 8.0 m for the San Mateo fault segments would produce seafloor uplift ranging from +6.91 m to -1.10 m peak-to-trough amplitude, which would produce runup of 6.75 m NAVD88 at SONGS. Therefore, the largest tsunami from the Coastal Fault System would be smaller than the Eastern Aleutian worst-case model above, but would still be larger than the largest tsunami from the postulated Palos Verdes fault zone scenario, discussed below.

c. Palos Verdes Fault Zone – Lasuen Knoll Section

The largest postulated earthquake from the Palos Verdes fault zone that has been modeled as the potential source of a tsunami at the SONGS site is a 3-segment source from the Lasuen Knoll section (Borrero et al, 2004). The Lasuen Knoll section at the southern end of the Palos Verdes fault zone is farther offshore than the Coastal Fault System, and is located about 28 km from SONGS. This modeled earthquake was an earthquake of Mw7.1, with average fault displacement of 4.0 m (5.0 m maximum). The maximum seafloor uplift (initial wave peak-to-trough) would range from +1.74 m to -1.20 m. The tsunami runup estimated at SONGS would be 3.75 m NAVD88.

Even assuming a worst-case Mw7.8 earthquake rupture from Santa Monica Bay to Lasuen Knoll (as postulated in the revised model), it would be a long, complex source that will focus tsunami energy shoreward in Santa Monica and San Pedro Bays, and offshore to the west, with local tsunami energy from the Lasuen Knoll segment directed to SONGS. The Palos Verdes source includes the Palos Verdes Hills, where the greatest uplift would be expected, but this would be located above sea level and would not contribute to tsunami generation. The seafloor uplift from the submerged areas in Santa Monica Bay, San Pedro Bay and San Pedro Basin would have lower wave amplitudes and would be expected to produce two major wave fronts, north and south of the Palos Verdes Peninsula. This pattern would resemble the model for the Mw7.6 Catalina tsunami scenario (Legg et al. 2004) which would produce a maximum runup at SONGS of about 3.75 m NAVD88.

The Palos Verdes largest postulated tsunami runup values are lower than the Mw7.62 Coastal Fault System tsunami and the Eastern Aleutians worst-case model (EA-sc3). In summary, the Eastern Aleutians subduction zone represents the most severe tsunami potential at SONGS, with 7.7 m tsunami elevation offshore and 8.67 m runup NAVD88.

Sincerely,

Hany Elwany, Ph.D.
Coastal Environments Inc.

REFERENCES:

Borrero, J.C., M.R. Legg, and C.E. Synolakis, 2004. Tsunami sources in the southern California Bight. *Geophysical Research Letters*, 31(13), L13211.

Coastal Environments, 2022a. Coastal Hazard, Step by step description of the modeling to evaluate the potential ground-shaking intensity associated with nine segments. Letter submitted to SCE dated 26 August 2022.

Coastal Environments, 2022b. Coastal Hazard Analysis At San Onofre Nuclear Generating Station, Tsunami Hazards, Submitted to Southern California Edison, 31 March, CE Ref. No. 22-04. 68 pp plus 1 Appendix.

Legg, M. R., C. E. Synolakis, and J. Borrero, 2004, Tsunami hazards associated with the Catalina Fault in southern California, *EERI Spectra, 20(3),* 1-34.

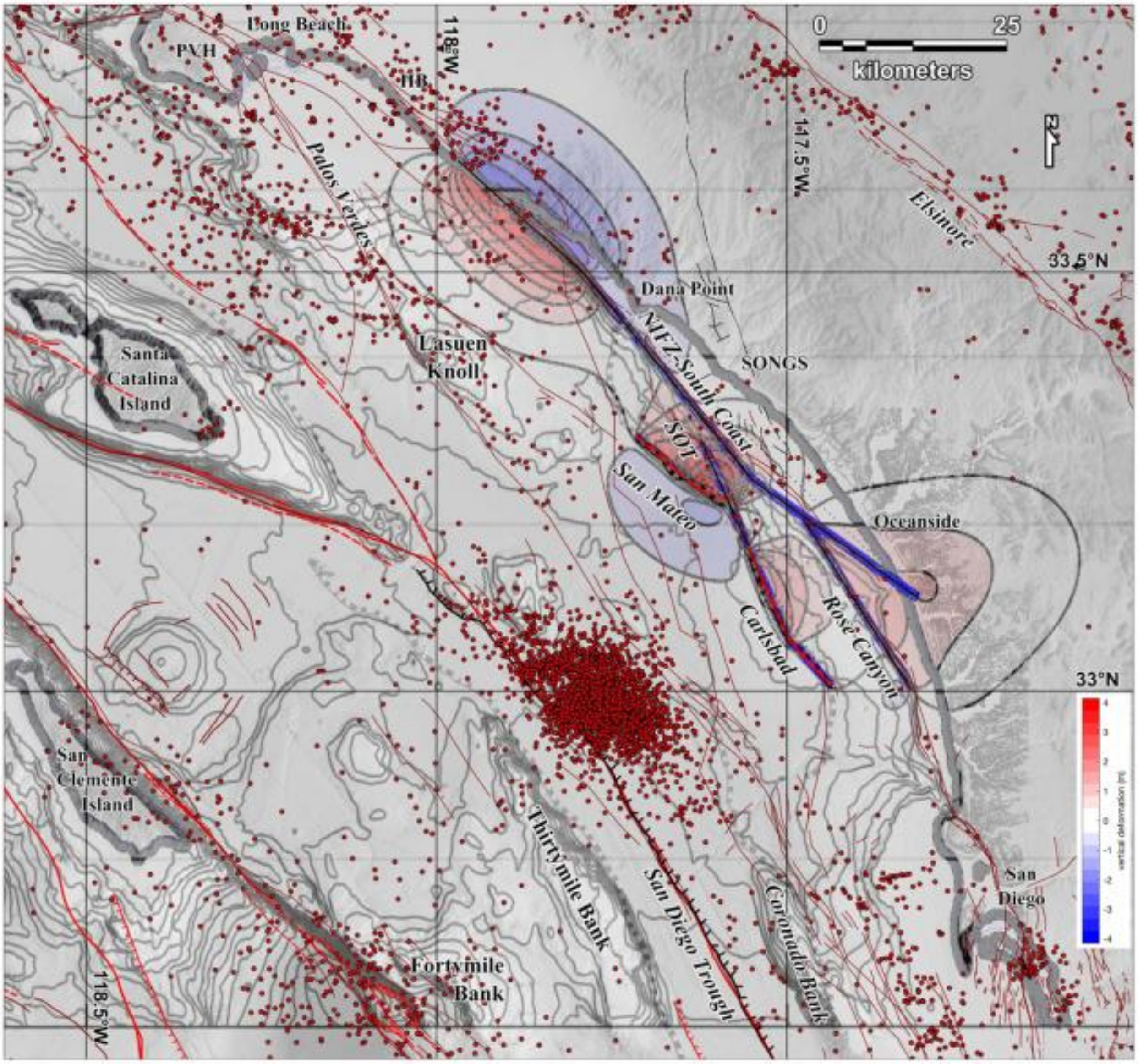

Figure 1. **Map showing seafloor deformation produced by local tsunami source 1 with all nine fault segments, bathymetry and relocated seismicity (M > 2, 1981-2019; Hauksson et al., 2012, 2019 update). Palos Verdes Fault is show including Lasuen Knoll. From Coastal Environments (CE, 2022b)**

Origin of the Palos Verdes Restraining Bend and Its Implications for the 3D Geometry of the Fault and Earthquake Hazards in Los Angeles, California

Franklin D. Wolfe*[1], John H. Shaw[1], and Andreas Plesch[1]

ABSTRACT

The Palos Verdes fault zone (PVFZ) extends across the southwestern Los Angeles basin and Inner Continental Borderland, California, and is considered capable of generating large ($M_w > 7$), damaging earthquakes with short recurrence intervals. The 110 km long fault zone is composed of vertical and moderately dipping segments that accommodate oblique, right-lateral reverse displacement. Onshore, there is a counterclockwise reorientation in the PVFZ's strike, which produces a major restraining bend that generates the Palos Verdes Peninsula. Here, we use well and seismic reflection data to develop kinematic models that show folding of the PVFZ by the Wilmington blind thrust led to formation of the restraining bend. North of the peninsula in Santa Monica Bay, debate persists over the extent, geometry, and activity of the PVFZ. Here, we analyze a dense grid of high-resolution seismic reflection data and present a new mapping of the Santa Monica Bay segment of the PVFZ, including multiple active splays (e.g., Redondo Canyon fault zone) that occur within a broad damage zone at the northern termination of the fault system. Based on these insights and prior studies, we develop a new, comprehensive 3D model of the PVFZ including its Santa Monica Bay, San Pedro Bay, and Lasuen Knoll segments. The sizes of these segments indicate that PVFZ is capable of larger events than previously reported —M_w 7.1–7.4 for single-segment ruptures and M_w 7.4–7.8 for multisegment ruptures. Based on a reported slip rate of 1.1–5.9 mm/yr, average recurrence intervals for these single- and multisegment rupture scenarios are 580–610 and 760–1170 yr, respectively.

KEY POINTS

- The Palos Verdes Peninsula formed due to structural imbrication by the underlying Wilmington blind thrust.
- We develop a new, comprehensive 3D representation of the Palos Verdes fault to assess seismic hazards.
- The size of the Palos Verdes fault suggests that it is capable of larger events than previously considered.

Supplemental Material

INTRODUCTION

The Los Angeles basin (LAB) and Inner Continental Borderland (ICB) are located in southern California between the Transverse and Peninsular Ranges (Fig. 1), and have undergone a polyphase deformational history driven by the relative motions of the Pacific–North America plate boundary, including a transition from extensional tectonics during the late Miocene (~7–4 Ma) to a transpressional tectonic regime during the Pliocene (initiating ~4 Ma) (Wright, 1991; Yeats and Beall, 1991; Crouch and Suppe, 1993; Atwater and Stock, 1998). Today, active strike-slip and reverse faults accommodate ~4–6 mm/yr of northeast-to-southwest-oriented contraction across the LAB and ~6–8 mm/yr of dextral shear within the ICB (Walls *et al.*, 1998; Argus *et al.*, 1999; Meade and Hager, 2005; Hauksson *et al.*, 2012; Yang and Hauksson, 2013). Faults in the region have produced numerous historical earthquakes with reverse, oblique, and strike-slip focal mechanisms (e.g., 1994 M_w 6.7 Northridge, 1987 M_w 6.0

1. Department of Earth and Planetary Sciences, Harvard University, Cambridge, Massachusetts, U.S.A., https://orcid.org/0000-0002-6680-7849 (FDW); https://orcid.org/0000-0002-3971-3812 (JHS); https://orcid.org/0000-0002-3355-9199 (AP)

*Corresponding author: wolfe_franklin@g.harvard.edu

Cite this article as Wolfe, F. D., J. H. Shaw, and A. Plesch (2022). Origin of the Palos Verdes Restraining Bend and Its Implications for the 3D Geometry of the Fault and Earthquake Hazards in Los Angeles, California, *Bull. Seismol. Soc. Am.* **112**, 2689–2714, doi: 10.1785/0120210278

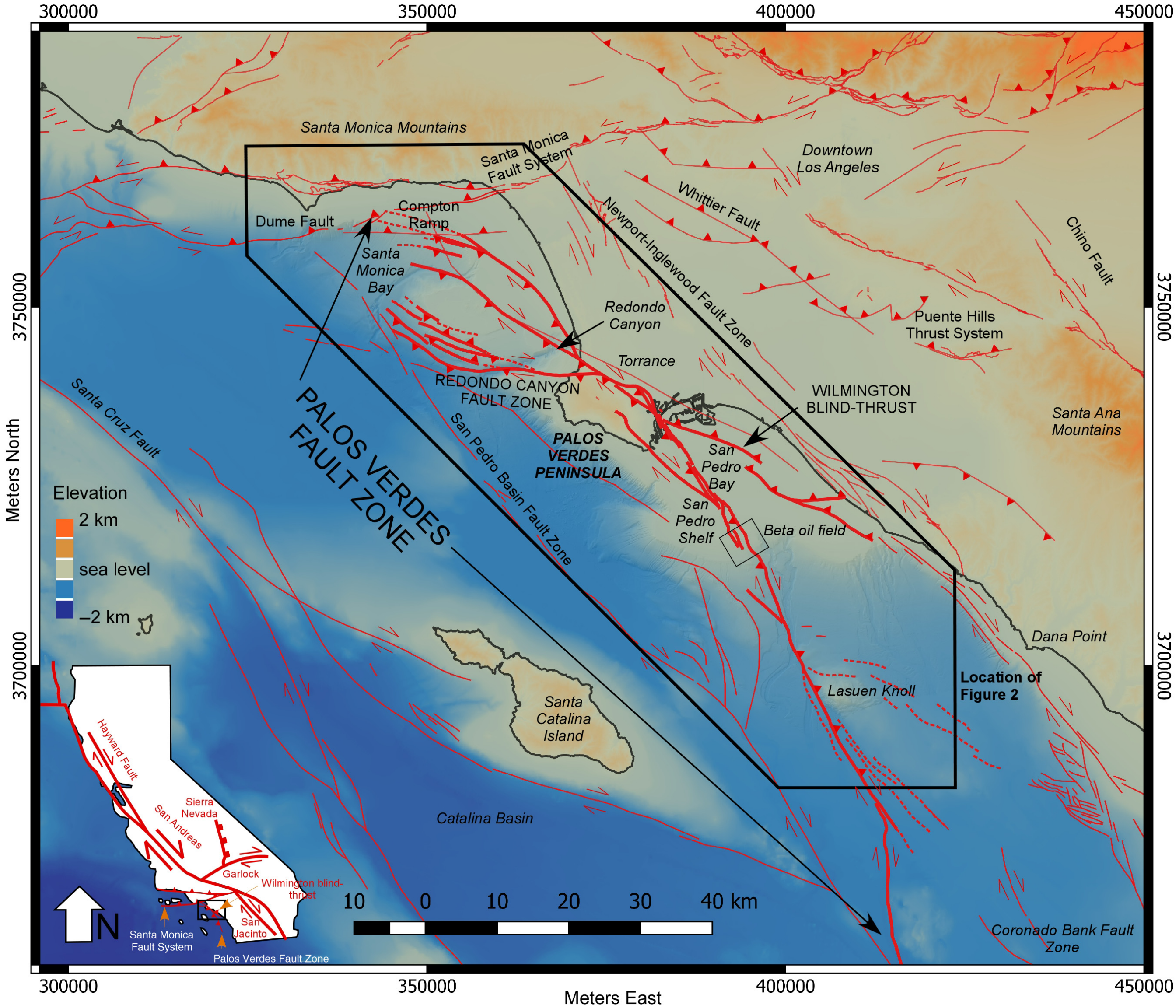

Figure 1. Regional location map showing the Palos Verdes fault zone (PVFZ) and other active structures in the Los Angeles basin (LAB) and Inner Continental Borderlands (ICBs). The trace of the PVFZ and Redondo Canyon fault zone (RCFZ) is from this study, Brankman and Shaw (2009), Goodman *et al.* (2015), and Brothers *et al.* (2015). The Wilmington blind-thrust (WBT) fault is from Wolfe *et al.* (2019), and other faults are from the U.S. Geological Survey (USGS) Quaternary Faults database (U.S. Geological Survey and California Geological Survey, 2006). Sense of slip is only shown on some of the major faults for simplicity. Bathymetry and elevation are color coded. The lower-left inset with an outline of California shows the tectonic context of the study region (black box) with only major regional faults shown. Map axes coordinates are shown in NAD27/UTM zone 11N (m). The color version of this figure is available only in the electronic edition.

Whittier Narrows, 1933 M_w 6.4 Long Beach), and pose the threat of additional events within highly populated and economically significant regions of the broader Los Angeles metropolitan area (Hauksson and Saldivar, 1986; Jones *et al.*, 1994; Dolan *et al.*, 1995; Shaw and Shearer, 1999; Hauksson, 2000; Plesch *et al.*, 2020).

The Palos Verdes fault zone (PVFZ) is one of the largest deterministic sources of seismic hazard in the Los Angeles region, and is composed of numerous fault segments and bends. The PVFZ lies along the southwestern margin of the basin, has a relatively fast slip rate (1.1–5.9 mm/yr; Table 1), and traverses through major industrial and port facilities (Stephenson *et al.*, 1995; McNeilan *et al.*, 1996; Brankman and Shaw, 2009; Brothers *et al.*, 2015). Onshore, a major restraining bend along the Palos Verdes fault generates the Palos Verdes Peninsula (Fig. 1)—one of the most prominent topographic features in Los Angeles (Wright, 1991; Ward and Valensise, 1994). Notably, this restraining bend occurs directly above where the mapped traces of the Palos Verdes fault override the recently documented Wilmington blind thrust (WBT; Wolfe *et al.*, 2019; Fig. 1).

TABLE 1
Compiled and Preferred Slip-Rate Estimates for the Palos Verdes Fault Zone

Study	Slip Rate (mm/yr)	Age Range	Segment(s)	Method
Ward and Valensise (1994)	3.0–3.7	2.4–3.0 Ma	All	Numerical fault modeling
Stephenson *et al.* (1995)	2.5–3.8	80–120 k.y.	San Pedro Bay (onshore)	Offset paleochannel
McNeilan *et al.* (1996)	2.7–3.0	7.8–8.0 k.y.	San Pedro Bay	Offset paleochannel
Rigor (2003)	1.8–5.9, 2.6–3.5	1.6–4.2 Ma, 3.0–3.6 Ma	San Pedro Bay	Offset depocenters
Meade and Hager (2005) (dextral strike-slip/uplift rates)	3.4 ± 1.4/3.1 ± 1.5	Active	All	Numerical modeling of GPS data
Cooke and Marshall (2006)	3.2	Active	All	Numerical fault modeling
Brankman and Shaw (2009) (dextral strike-slip/oblique slip rate)	3.3 ± 0.3/4.0 ± 0.3	~1.5 Ma	San Pedro Bay	Offset basin margins and seismic mapping
	3.3 ± 0.3/4.0 ± 0.3		Lasuen Knoll	
Sorlein *et al.* (2013)	1.1–1.6	~3.0 Ma	San Pedro Bay (onshore)	Uplifted geomorphic features and patterns of sedimentation and erosion
Brothers *et al.* (2015)	1.3–2.8	31 k.y.	Lasuen Knoll	Offset geomorphic features
Goodman *et al.* (2015)	3.08	125 k.y.	San Pedro Bay (onshore)	Offset paleochannel
This study	1.1–5.9	~1.5 Ma	All	Combination of previously published rates

Fault bends and segment linkages, such as those along the PVFZ, may have a significant impact on the size and extent of ruptures (e.g., 2010 M 7.2 El Mayor–Cucapah [Wei *et al.*, 2011] and 2016 M 7.8 Kaikōura [Hamling *et al.*, 2017; Litchfield *et al.*, 2018] earthquakes), and thus directly impact earthquake hazards (Hamling *et al.*, 2017; Litchfield *et al.*, 2018). Natural and experimental data show that in strike-slip settings, regardless of scale, strike-slip faults commonly initiate as en echelon fault and fold segments that link together as displacement increases (Tchalenko, 1970; Wilcox *et al.*, 1973; Cunningham and Mann, 2007). Fault bends often represent areas where fault segments are linked across segments, and their origins reflect fault kinematics, stress patterns, and possible feedbacks between climate, topography, and tectonics (Cunningham and Mann, 2007). Understanding the ability of these geometric segment boundaries to both inhibit and form barriers to earthquake propagation between multiple segments of a fault system is an area of active research (Sibson, 1985; Lozos *et al.*, 2012; Douilly *et al.*, 2015; Elliott *et al.*, 2015). Our study seeks to provide a comprehensive understanding of the geometric complexities of PVFZ to support such assessments.

We integrate data from multiple sources (e.g., 2D and 3D seismic reflection data, published cross sections, and petroleum and water wells) to build a 3D model of the interaction between the PVFZ and WBT to investigate the origin of the Palos Verdes Peninsula and its associated restraining bend. Specifically, we employ 2D and 3D kinematic modeling approaches to show how the growth of the Wilmington anticline, which is located above the WBT and in the footwall of the Palos Verdes fault, deforms the Palos Verdes fault. This process steepens the Palos Verdes fault and produces a counterclockwise rotation in its surface trace that is consistent with observations in both surface and subsurface data (Stephenson *et al.*, 1995; McNeilan *et al.*, 1996; Goodman *et al.*, 2015).

Based on our new understanding of the Palos Verdes restraining bend, we develop a comprehensive 3D model describing the subsurface geometry of the fault including its northern and southern extensions in Santa Monica and San Pedro Bays, respectively (Fig. 1). North of the Palos Verdes Peninsula in Santa Monica Bay, many aspects of the fault's geometry and kinematics are unresolved (Nardin and Henyey, 1978; Bohannon *et al.*, 2004; Fisher *et al.*, 2004b). Building on prior work (e.g., Bohannon *et al.*, 2004), we investigate the detailed structure of the Palos Verdes fault in this region using a dense grid of high-resolution seismic reflection data. Our mapping shows that the main strand of the Santa Monica Bay segment of the PVFZ consists of a moderately southwestward-dipping fault with high-angle hanging-wall splays, similar to its recent mapping in the San Pedro Bay and onshore (Brankman and Shaw, 2009; Goodman *et al.*, 2015). In addition, we map numerous northwest-trending branching splays of the Palos Verdes fault, including the Redondo Canyon fault zone (RCFZ). Correlation of these faults with seafloor traces (Bohannon *et al.*, 2004) suggest that several have recent activity and thus should be considered in seismic hazard assessments.

We combine our analysis of faults within Santa Monica Bay and the onshore peninsula with results from prior studies that have documented the fault geometry in San Pedro Bay (Bryant and Raub, 1986; Kelsch, 1996; McNeilan *et al.*, 1996; Marlow *et al.*, 2000; Bohannon *et al.*, 2004; Fisher *et al.*, 2004b; Brankman and Shaw, 2009) to build a new comprehensive 3D model for the Palos Verdes fault. This model differs from that used in current community fault models (CFMs) and seismic hazard assessments (Field, 2000; Plesch *et al.*, 2007), which does not include the full extent or detailed fault zone geometry described herein and by others (McNeilan *et al.*, 1996; Brankman and Shaw, 2009; Brothers *et al.*, 2015; Goodman *et al.*, 2015). Our new model illustrates that the PVFZ is a long,

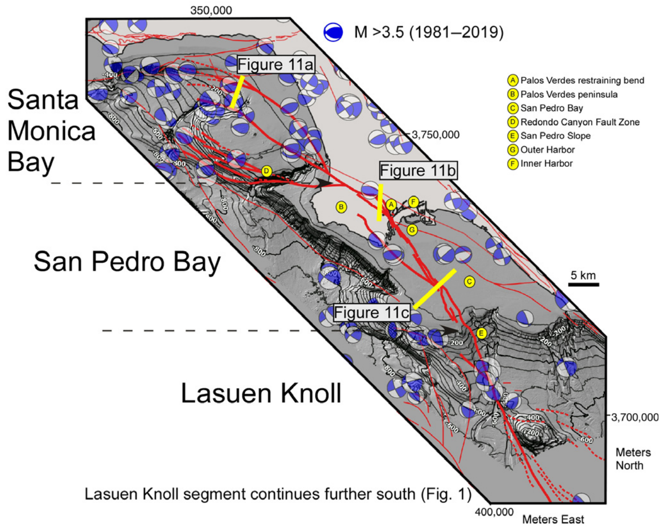

Figure 2. Regional seismicity and segments of the PVFZ. Focal mechanisms from Yang *et al.* (2012) and Hauksson *et al.* (2012). The locations for the cross sections in Figure 11 are shown as yellow lines. Map axes coordinates are shown in NAD27/UTM Zone 11N (m). The color version of this figure is available only in the electronic edition.

continuous structure with multiple segments that exhibit complex geometries and kinematics, and thus might be expected to rupture in both single or multisegment earthquakes. We explore a range of potential earthquake rupture scenarios with forecast magnitude and recurrence intervals developed based on empirical relations with rupture area (Hanks and Bakun, 2002, 2008), average displacement (Biasi and Weldon, 2006; Thingbaijam *et al.*, 2017), and previously documented slip rates (Brankman and Shaw, 2009; Brothers *et al.*, 2015; Goodman *et al.*, 2015). Our analysis indicates that the PVFZ is capable of larger magnitude earthquakes (M_w 7.1–7.4 and M_w 7.4–7.8 for single- and multisegment ruptures, respectively) than the previously suggested (e.g., Brankman and Shaw, 2009), and that the Santa Monica Bay segment and RCFZ should be considered as active seismic sources capable of moderate-to-large magnitude earthquake events that would directly impact the metropolitan Los Angeles area.

The body of the article is organized as follows: First, we describe the geometry and kinematics of each major segment of the PVFZ (San Pedro Bay, Santa Monica Bay, and Lasuen Knoll). Next, we present a new comprehensive model of the PVFZ, which includes the full extent and detailed geometry described in the first section. Finally, we calculate single and multisegment rupture scenarios, including earthquake magnitudes and recurrence intervals, for the PVFZ based on our new comprehensive fault model.

THE PVFZ

The PVFZ has long been considered a major tectonic element in the western margin of the LAB (Woodring *et al.*, 1946). The map trace of the fault zone extends for more than 110 km offshore from the northern part of the Santa Monica Bay, onshore below the Palos Verdes Peninsula, and offshore beneath the San Pedro Bay, the San Pedro Shelf, and deep water area near Lasuen Knoll (Fig. 1; Woodring *et al.*, 1946; Yerkes *et al.*, 1965; Fisher *et al.*, 1987; Greene and Kennedy, 1987; Wright, 1991; Stephenson *et al.*, 1995; McNeilan *et al.*, 1996; Brankman and Shaw, 2009; Brothers *et al.*, 2015). The mapped fault zone is more than 2 km wide at some localities and composed of numerous anastomosing traces, which produce local restraining and releasing bends along strike (McNeilan *et al.*, 1996; Brankman and Shaw, 2009).

The PVFZ originated as a normal fault in the late Miocene (~7 Ma) and was reacted in the Pliocene as an oblique, right-lateral reverse fault (Brankman and Shaw, 2009). Today, it is generally considered the fastest slipping fault in the LAB (Ward and Valensise, 1994; Stephenson *et al.*, 1995; McNeilan *et al.*, 1996; Rigor, 2003; Meade and Hager, 2005; Cooke and Marshall, 2006; Brankman and Shaw, 2009). Many authors document evidence of Late Pleistocene slip on this fault system (Fisher *et al.*, 1987; Stephenson *et al.*, 1995; McNeilan *et al.*, 1996; Brankman and Shaw, 2009; Goodman *et al.*, 2015), and a zone of distributed seismicity is observed surrounding its mapped fault trace (Hauksson and Saldivar, 1989; Hauksson *et al.*, 2012; Yang *et al.*, 2012; Ross *et al.*, 2019; Fig. 2). Previous deterministic seismic hazard assessments suggest that single or multisegment ruptures of the PVFZ could produce M_w 6.6–6.9 and M_w 7.1–7.3 earthquakes, respectively. These would pose significant hazard to the metropolitan Los Angeles region, which sits above a deep sedimentary basin that tends to amplify seismic waves (Field, 2000; Olsen, 2000). Given the offshore extent of the fault, it might be capable of generating local tsunamis in the San Pedro and Santa Monica Bay, as well as in the Los Angeles and Long Beach Harbors (Bohannon and Gardner, 2004).

The geometry, sense of slip, and extent of the PVFZ have been debated (McNeilan *et al.*, 1996; Fisher *et al.*, 2004b; Brankman and Shaw, 2009; Brothers *et al.*, 2015; Goodman *et al.*, 2015). Some suggest the PVFZ is a moderately southwest-dipping oblique, reverse, right-lateral fault (Davis *et al.*, 1989; Shaw and Suppe, 1996; Shaw and Shearer, 1999; Brankman and Shaw, 2009). Others have documented primarily dextral strike-slip motion and interpret the fault as a high-angle strike-slip fault with variable dip (60°–90°) (Junger and Wagner, 1977; Nardin and Henyey, 1978; Wright, 1991; Ward and Valensise, 1994; McNeilan *et al.*, 1996; Bohannon and Geist, 1998; Fisher *et al.*, 2004b). There is a general agreement that both dextral strike-slip and reverse dip-slip motion exists along segments of the PVFZ and that restraining and releasing beds are responsible for prominent vertical displacements, such as the uplift of the Palos Verdes Peninsula onshore and the offshore Beta oil field anticline (Darrow and Fischer, 1983; Freeman *et al.*, 1987; Ward and Valensise, 1994; Kelsch, 1996; Brankman and Shaw, 2009; Fig. 1).

The PVFZ has previously been described relative to its main geographic segments (Brankman and Shaw, 2009; Brothers *et al.*, 2015). Here, we define the PVFZ relative to three geographic and structural segment boundaries where major changes in geometry and fault zone kinematics are observed: the Lasuen Knoll, San Pedro Bay, and Santa Monica Bay segments (Fig. 2). Because of the major changes in geometry and fault zone kinematics that occur at the boundaries between these segments, they may impact the size and extent of earthquake ruptures (Brankman and Shaw, 2009). Thus, we will consider these segment boundaries as part of the rupture scenarios described in our seismic hazard assessment.

Our analysis begins with the San Pedro Bay segment, where we present a model for the Palos Verdes restraining bend and uplift of the Palos Verdes Peninsula. These insights are combined with the previous work (Bohannon *et al.*, 2004; Fisher *et al.*, 2004b; Brankman and Shaw, 2009; Brothers *et al.*, 2015) to develop a new, 3D model of the PVFZ beneath the peninsula and extending south into San Pedro Bay (Figs. 1, 2). Next, we describe our analysis of the Santa Monica Bay segment, which builds on Bohannon *et al.* (2004) and includes a new mapping of the RCFZ. Finally, we rely on previous investigations (e.g., Brankman and Shaw, 2009; Brothers *et al.*, 2015) to represent the Lasuen Knoll segment, which together with the San Pedro and Santa Monica Bay segments is integrated into a new, comprehensive 3D model of the PVFZ.

San Pedro Bay segment

Fault zone geometry and kinematics. The San Pedro Bay segment of the PVFZ extends over 60 km along-strike south from the San Pedro slope to the onshore Palos Verdes Peninsula (Fisher *et al.*, 1987; Greene and Kennedy, 1987; Marlow *et al.*, 2000; Fig. 2). Offshore, the near-surface fault zone is up to 2 km in width in some localities (Fig. 2). The fault zone is comprised of numerous overlapping and anastomosing, near-vertical fault splays, some of which produce right-lateral stepovers and linear seafloor scarps that reach up to 400 m in height and are indicative of Holocene fault rupture (Fisher *et al.*, 2004a).

Previous investigations of 3D seismic reflection data suggest that these near-surface splays merge at depth (~3 km) into a moderately southwest-dipping fault (40°–70°) that resolves up-to-the-west relative motion (Brankman and Shaw, 2009). The degree of contractional folding increases northward from the San Pedro Slope, and the fault separates heavily deformed Miocene and Pliocene strata to the west from relatively flat-lying upper Pliocene and Quaternary strata to the east. An anticline of the western side of the fault produces the structural trap for the Beta oil field (Fisher *et al.*, 1987; Kelsch, 1996; Fisher *et al.*, 2004a; Brankman and Shaw, 2009).

The structure within the Beta oil field imaged in 3D seismic reflection data contains Miocene strata that thicken eastward toward the fault (Brankman and Shaw, 2009). This pattern is indicative of growth strata and has been interpreted as evidence that the San Pedro Bay segment of the PVFZ initiated as a normal fault during the late Miocene (Brankman and Shaw, 2009). Evidence for rifting during this time period is widespread in the Inner Borderlands and LAB associated with oblique crustal extension due to clockwise rotation of the Transverse Ranges and opening of the Inner California Borderlands (Luyendyk, 1991; Crouch and Suppe, 1993; Nicholson *et al.*, 1994; Atwater and Stock, 1998; Bohannon and Geist, 1998; Brankman and Shaw, 2009). The PVFZ was subsequently inverted in the late Pliocene to early Pleistocene, forming the modern, oblique, reverse right-lateral system that is active today. Together, the fault geometry, stratigraphic offsets of basement to Pliocene stratigraphy demonstrating reverse slip, and an offset early Holocene paleochannel on the western side of the PVFZ near the location of the Beta oil field demonstrate dextral strike slip on the fault at a rate of 3.3 ± 0.3 mm/yr over the last ~1.5 Ma. Including the reverse component of displacement yields a right-lateral oblique reverse slip rate of 4.0 ± 0.3 mm/yr (Brankman and Shaw, 2009; Table 1).

Within the Outer Harbor (Fig. 2), the PVFZ has an average strike of N40W. The down-dip geometry of the PVFZ is poorly constrained, but the near-surface fault zone is 100–300 m wide and is composed of numerous anastomosing strands (McNeilan *et al.*, 1996). These strands are near vertical to steeply dipping to the west with up-to-the-west separation. Vertical separation across the fault is evidenced in the near-surface Holocene sediments along most of the main fault trace. Buried Holocene stream channels that are offset by 21–24 m resolve a right-lateral strike-slip rate of 2.7–3.0 mm/yr beneath the Outer Harbor over the past 7.8–8 ka (McNeilan *et al.*, 1996; Table 1).

Within the Inner Harbor to onshore transition (Fig. 2), the PVFZ undergoes a major change in strike from N40W to N65W (Wright, 1991; Kelsch, 1996; Fig. 3), producing a restraining bend architecture at the location of the Palos Verdes Peninsula. Onshore, the structure of the Palos Verdes Peninsula is a doubly plunging anticline with an emergent portion that measures 15 km in length, 8 km in width, and 400 m in height above sea level. Well and seismic reflection data show that the anticline extends offshore and, thus, is at least twice as large with three times the structural relief as the onshore surface expression (Ward and Valensise, 1994; Brankman and Shaw, 2009). Deformed strata of early to late Pleistocene age are present along the northeastern flank of the Palos Verdes Hills, and as much as 1.8 km of west-side-up vertical separation is observed on the Lower Cretaceous Catalina Schist basement across the fault zone within oil wells and high-resolution seismic reflection data. The schist is generally displaced on top of Pliocene–Miocene stratigraphy

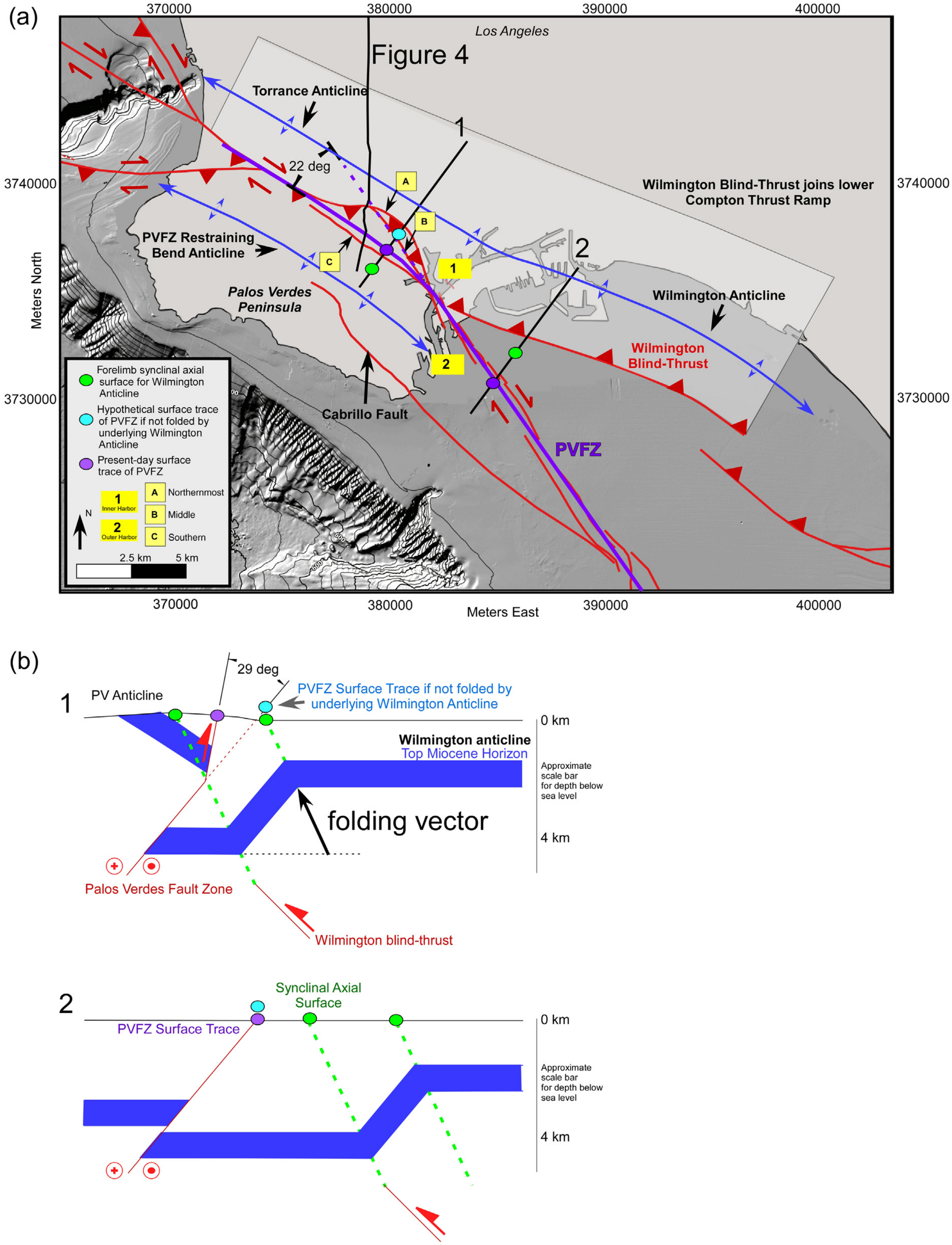

Figure 3. Map- and cross-section-based schematic model of the PVFZ and Wilmington anticline interaction. (a) Where the WBT fault and PVFZ converge onshore, the PVFZ undergoes a counterclockwise rotation and reorients in a more northwesterly direction. The main splays of the PVFZ onshore are labeled with yellow indicators. Map axes coordinates are shown in NAD27/UTM zone 11N (m). (b) The map-based rotation is due to imbrication of the PVFZ by the underlying WBT fault, where the PVFZ is located directly above the forelimb of the Wilmington anticline. The effecct of imbrication on the hanging-wall stratigraphy of the PVFZ is not demonstrated for simplicity. Only an approximate vertical scale bar is provided here for this conceptual model. The color version of this figure is available only in the electronic edition.

(Woodring *et al.*, 1946; Schoellhamer and Woodford, 1951; Yerkes *et al.*, 1965; Goodman *et al.*, 2015).

Onshore where the PVFZ reorients from N40W to N65W, a ~1.7 km wide near-surface fault zone is present and contains at least three active faults (Fig. 3) that have been imaged in high-resolution seismic reflection profiles and interpreted from aerial imagery (Stephenson *et al.*, 1995; Goodman *et al.*, 2015). The northernmost splay (labeled A in Fig. 3) forms a blind reverse fault with a tipline well constrained at depth by horizons that can be traced continuously through the syncline near the fault tip. At the surface, no discernable lateral offset is observed where an abandoned channel crosses this splay. Pliocene strata in the hanging wall of this fault splay thin to the southwest toward the Palos Verdes anticlinorium, indicative of the modern transpressional slip interpreted on PVFZ (Goodman *et al.*, 2015).

The middle and southern splays (labeled B and C, respectively, in Fig. 3) are steeply dipping (75°–85°), reverse, right-lateral oblique faults that accommodate the motion on the PVFZ and offset the basement reflector at depth (Goodman *et al.*, 2015). These splays cut youthful paleochannel features at the surface, yielding an estimated ~3.08 mm/yr of right-lateral slip rate over the last ~125 ka (Goodman *et al.*, 2015). This is consistent with the long-term estimates by Ward and Valensise (1994) of slip rate on a southwest-dipping oblique reverse fault of 3.0–3.7 mm/yr.

Together, the three onshore splays document the partitioning of slip in the upper crust on both strike-slip and reverse faults within the PVFZ. This fault architecture is very similar to that proposed by Brankman and Shaw (2009) for the San Pedro Bay segment imaged in 3D seismic reflection data offshore, which imaged a moderately west-dipping basal fault ramp with numerous high-angle splays in its hanging wall. In addition, numerous wells located in the forelimb of the Palos Verdes anticline (Wright, 1991; Shaw and Suppe, 1996; Goodman *et al.*, 2015) suggest that Miocene strata are thick in the hanging wall of the onshore portion of the PVFZ, which is also similar to the architecture previously described for the San Pedro Bay segment (Brankman and Shaw, 2009). These observations, as well as the continuous trace along the entire extent of the San Pedro Bay segment, motivate our approach to consider the onshore portion of the PVFZ as part of the San Pedro Bay segment.

Origin of the PVFZ restraining bend. The Palos Verdes restraining bend occurs where the PVFZ crosses the trace of the WBT in map view (Fig. 3; Wright, 1991; Shaw and Suppe, 1996; Wolfe *et al.*, 2019). Along this juncture at depth, the west-dipping PVFZ cuts up from the footwall to the hanging wall of the WBT fault across the forelimb of the Wilmington anticline (Fig. 4). Both the PVFZ and WBT fault initiated as late Miocene normal faults and reactivated as Pliocene transpressional structures that remain active today. The sense of displacement on both the structures is consistent with the present-day stress field where the maximum horizontal compressive stress is oriented northeast–southwest across the western LAB (Hauksson, 1990; Brankman and Shaw, 2009; Wolfe *et al.*, 2019). Thus, the Pliocene to recent growth of the underlying Wilmington anticline would be expected to fold the overlying portion of the PVFZ, and thus influence its dip and map trace. In this section, we use kinematic modeling approaches to test: (1) whether the growth of the Wilmington anticline is a feasible mechanism to explain the existence and location of the PVFZ restraining bend and (2) whether the down-dip geometry of the PVFZ has an impact on the cross sectional and/or map pattern orientation of the PVFZ once it is folded by the growth of the underlying Wilmington anticline.

Kinematic model setup and boundary conditions. To explore if folding of the Palos Verdes fault by the underlying Wilmington anticline is consistent with the mapped traces of the faults and geometry of the restraining bend, we developed a structural model based on geometric and kinematic balancing constraints (Fig. S1, available in the supplemental material to this article). Our forward modeling method conserves area during deformation and applies strain from the underlying fold (Wilmington anticline) to warp the overlying structure (Palos Verdes fault) (Hamblin, 1965; Groshong, 1990; Novoa *et al.*, 2000). Deformation in the Wilmington anticline is modeled with inclined shear deformation described by folding vectors, which are parallel to the axial surfaces that bound the forelimb of the Wilmington anticline and applied to describe the change in shape of the Palos Verdes fault. Application of inclined shear restoration or folding vectors to model deformation in 2D is widespread (Shaw *et al.*, 1999; Corredor *et al.*, 2005; Shaw, Novoa, and Connors, 2005; Lingrey and Vidal-Royo, 2015; Connors *et al.*, 2021). We extend these methods to 3D by assuming plane strain (Buddin *et al.*, 1997; Rouby *et al.*, 2000; Bjorklund and Burke, 2002; Griffiths *et al.*, 2002; Shackleton and Cooke, 2007; Guzofski *et al.*, 2009; Chenghua *et al.*, 2015). Thus, our 3D model is inherently 2.5D and seeks only to describe the folding of the PVFZ by the WBT, not to address oblique slip on the PVFZ and associated folding in its hanging wall.

We implemented our model using 2D and 3D geometric and kinematic analysis tools in Petroleum Experts MOVE software. To begin, we built 3D representations of the Wilmington anticline and PVFZ using the approach of Plesch *et al.* (2007) that are consistent with the current knowledge of the two structures defined by their mapped traces and subsurface geometries (McNeilan *et al.*, 1996; Brankman and Shaw, 2009; Goodman *et al.*, 2015; Wolfe *et al.*, 2019). For the Wilmington anticline, offshore 3D seismic reflection imagery and oil wells in the region define a broad northeast-dipping backlimb (~14°–20°) and a steeply dipping forelimb (~50°–60°) (Wolfe *et al.*, 2019). Onshore, seismic reflection profiles across the crest of the structure, along with well-based sections and oil

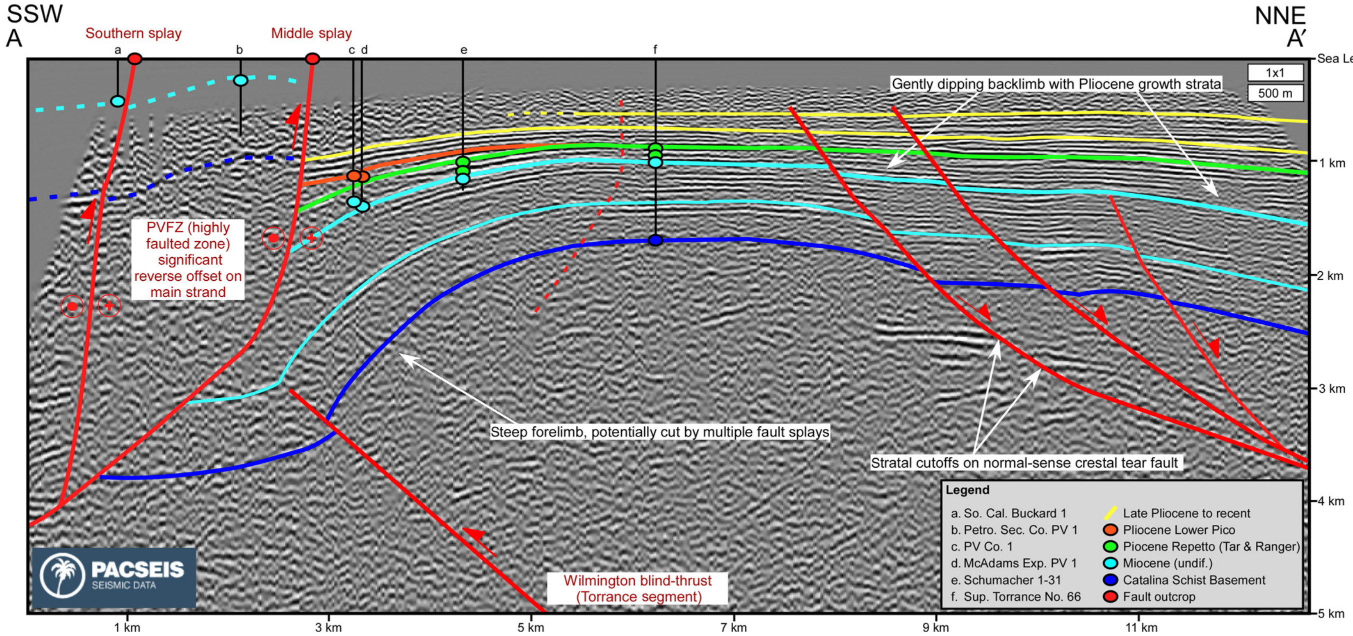

Figure 4. The Torrance anticline. Interpreted seismic reflection line tied to oil wells demonstrating the steep forelimb of the Torrance anticline located directly in the footwall of the PVFZ. The overal morphology of the anticline is consistent with the forelimb of the Wilmington anticline imaged offshore in 3D seismic reflection data and suggests these are continuous features (Wolfe *et al.*, 2019). The location of this seismic reflection line is shown in Figure 3. The location of the Main and Southern splays are tied to the surface traces of the faults. The color version of this figure is available only in the electronic edition.

field maps, reveal a similar geometry within the Torrance anticline (Fig. 4), which is the along-strike extension of the Wilmington anticline. Our 3D model of the Wilmington anticline is constrained by hundreds of well penetrations, oil field maps, and regional cross sections (Fig. 5).

Wolfe *et al.* (2019) documented that the Wilmington anticline is a southwest-vergent fault-propagation fold best described by Trishear folding kinematics. The front limb of the Wilmington anticline, which underlies the Palos Verdes fault beneath the peninsula (e.g., Fig. 4), has bed dips of ∼50°–60° southwest and has Pliocene growth strata that show evidence of both fold development by limb rotation and kink-band migration (Mitra, 1990; Suppe and Medwedeff, 1990; Erslev, 1991; Suppe *et al.*, 1992; Allmendinger, 1998; Shaw, Connors, and Suppe, 2005). This motivates our choice of the inclined shear deformation method to simulate the growth of the Wilmington anticline in the kinematic models (Figs. 6–8). In general, inclined shear restoration works well for approximations of restored geometries for folds developed by limb rotation and some more complex folding mechanisms (e.g., Trishear) (Novoa *et al.*, 2000).

We cannot directly observe the folding vector field, so we must constrain it in a geologically reasonable way (Novoa *et al.*, 2000) and test a range of possible orientations. The choice of an inclined shear (or folding vector) orientation must satisfy two basic requirements for choosing the restoration vector fields: (1) the restoration must satisfy appropriate balancing constraints (e.g., conserves area in 2D and volume in 3D), and (2) the restored or modeled profiles must be geologically reasonable (e.g., match a reasonable initial and final configuration defined by our Wilmington anticline model). These conditions are generally met when selecting a folding vector that is parallel to the axial surfaces within a structure (Novoa *et al.*, 2000). In the case of the Wilmington anticline forelimb, axial surfaces do not bisect the interlimb angles so models using restoration vectors will conserve area but not bed thickness during deformation. This is consistent with interpretation of the Wilmington anticline as a Trishear fold (Wolfe *et al.*, 2019), which forms by distributed shear within a triangular zone that expands outward from the fault tip and ensures that cross sectional area is conserved, but not bed thickness or length (Erslev, 1991; Allmendinger *et al.*, 2004; Shaw, Connors, and Suppe, 2005; Hardy and Finch, 2007).

Within the 3D offshore seismic reflection data, we measured the dip of the axial surfaces (∼40°–60°) bounding the forelimb of the Wilmington anticline, including the synclinal axial surface pinned to the tip of the WBT fault. This provides a range of inclined shear orientations that we will test in our model. These orientations, combined with the geometry of folded horizons in the forelimb of the Wilmington anticline, provide the information needed to describe the deformation of the overlying Palos Verdes fault. In 3D, the azimuth of the inclined shear vector is defined as being perpendicular to the strike of the Wilmington anticline (Hauksson, 1990; Fig. S1).

Our representation of the PVFZ prior to folding by the Wilmington structure is a simple, southwest-dipping planar fault that extends along a trace compiled from multiple investigators who mapped the structure in the San Pedro Shelf, Outer

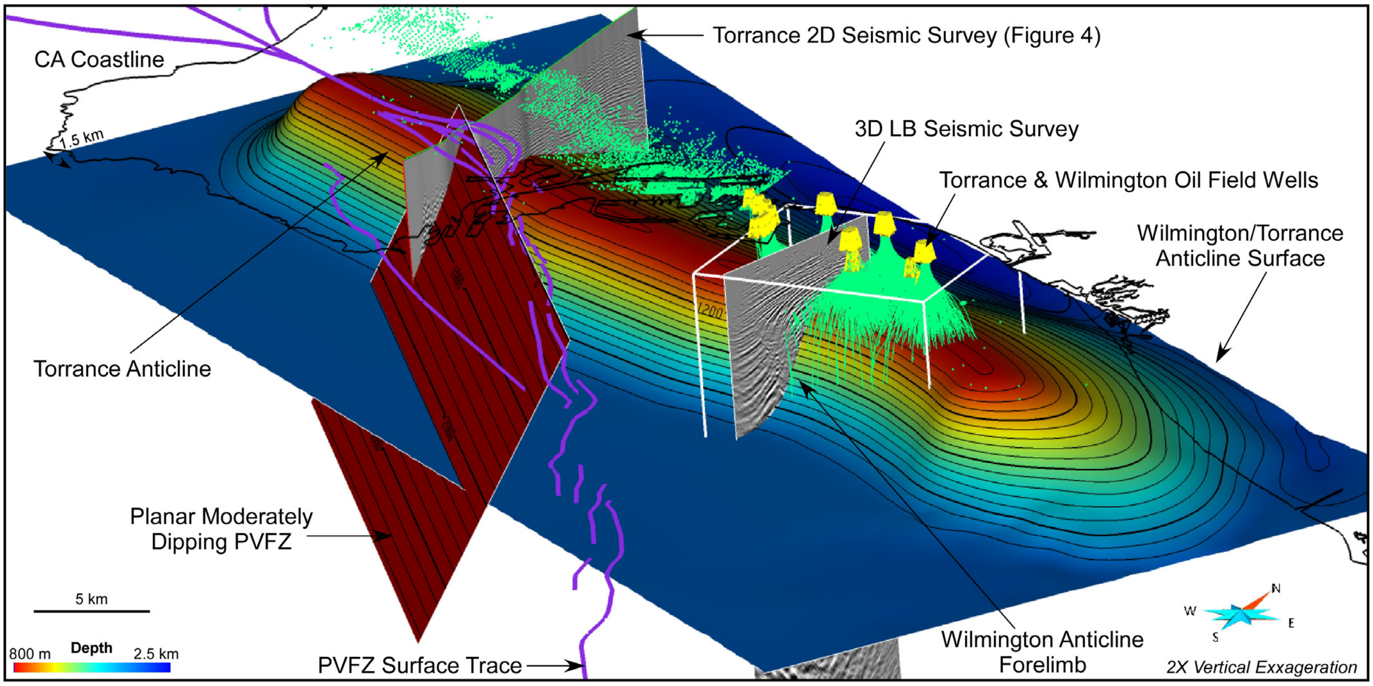

Figure 5. The 3D model of the PVFZ and Wilmington anticline interaction. Within this region, the steep forelimb of the Wilmington anticline occurs in the footwall of the PVFZ. Data constraints used to build the model are as follows: seismic data sources (Long Beach 3D Seismic Survey and PacSeis 2D Seismic Line), well data (CalGEM database), and fault and horizon maps (Wright, 1991; Otott *et al.*, 1996; Brankman and Shaw, 2009; Wolfe *et al.*, 2019). Vertical scales are provided by depth contours on the PVFZ and Wilmington and Torrance anticline surfaces. The color version of this figure is available only in the electronic edition.

Harbor, Inner Harbor, and onshore (Stephenson *et al.*, 1995; McNeilan *et al.*, 1996; Brankman and Shaw, 2009; Goodman *et al.*, 2015; Fig. 5). This planar representation of the Palos Verdes fault will be deformed in our model by the growth of the Wilmington anticline. Given the uncertainties in the geometry of the PVFZ at depth, we investigate a broad range of possible initial dips for the geometry of the fault (40°–70°) that encompass those proposed by prior studies (Fisher *et al.*, 2004b; Brankman and Shaw, 2009; Goodman *et al.*, 2015). Exploring a range of possible geometries of the PVFZ helps us to determine whether fault dip has a first-order impact on the degree of map view rotation or cross-sectional dip change of the PVFZ when folded by the underlying structure. We note that our modeling is not intended to define the dip of the fault at depth but rather to assess if folding of the PVFZ by the Wilmington structure is consistent with the surface trace and dip observations despite uncertainties in the fault geometry.

At stage one of our kinematic models, we assume horizontal strata in the location of the Wilmington anticline prior to the initiation of reverse slip on the fault in the late Pliocene (Fig. 6; Fig. S1). This is consistent with late Miocene to early Pliocene strata that maintain thickness across the fault, indicating they were deposited during a period of local tectonic quiescence (Wolfe *et al.*, 2019). Next, we model the growth of the Wilmington anticline using inclined shear deformation with a range of folding vector dip angles to its present-day geometry. Within the MOVE 2D and 3D Kinematic Unfolding workflows, we defined the present-day geometry of the Wilmington anticline as the target horizon, our flat horizon as the object to be deformed by the velocity field defined by the folding vector, and the Palos Verdes fault as a passive object to be folded (Fig. S1).

We emphasize that our analysis is focused on the region where the change in orientation of the PVFZ map trace occurs, and thus it seeks to explain the origin of the restraining bend but not the geometry of the northern extension of the fault in Santa Monica Bay. This northern extension of the fault may have formed by the propagation of the San Pedro segment to the north subsequent to it being deformed by interaction with the Wilmington structure. Alternatively, these northern fault segments may have formed independently. Given the nature of our geometric model, we cannot distinguish between these alternatives.

Kinematic model results. The 2D kinematic modeling results demonstrate that the growth of the Wilmington anticline deforms the overlying Palos Verdes fault, which steepens it dip through this process. The precise amount of the dip change depends on the initial fault geometry. With a starting dip of 45°, which corresponds to the preferred value from Brankman and Shaw (2009), the Palos Verdes fault is expected to steepen to a dip of 70°–80° (Fig. 6). Over the full range of starting dips that we consider (40°–70°), the PVFZ steepens to (65°–90°). This steep, near-surface dip of the fault is consistent

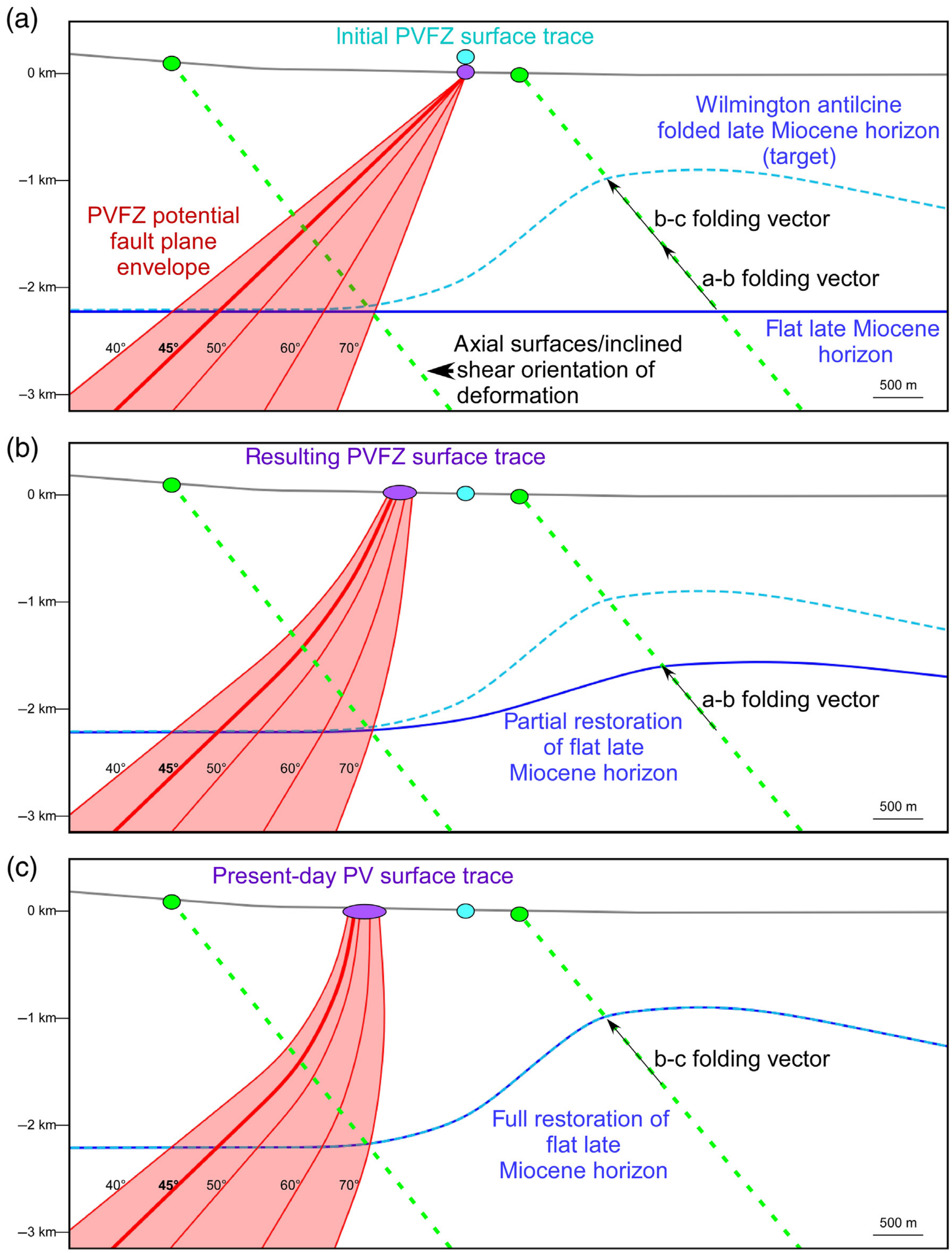

Figure 6. The 2D kinemaitc modeling of the evolution of the Palos Verdes (PV) restraining bend. (a) Initial model setup, including annotated folding vector and prefolding flat Miocene horizon and planar PVFZ. Multiple initial dips for the PVFZ are shown and consistent with previous assessments of the San Pedro Bay segment (Brankman and Shaw, 2009). The preferred dip 45° is shown as a bold red line. The green dashed lines represent the dip of the velocity field in this modeling procedure. These are the orientations of the axial surfaces measured to bound the forelimb of the Wilmington anticline. The dashed blue line represents the target of the forward modeling procedure carried out in Petroleum Experts MOVE Software. The Miocene horizon is not shown to be offset by the PVFZ here for simplicity. The goal of the model is to document the growth of the Wilmington anticline and its effect on the geometry of the PVFZ. (b) Intermediate steps demonstrating the progressive folding of the PVFZ and growth of the Wilmington anticline. (c) Final outcome, demonstrating the steep, uppermost segments of the folded PVFZ and significant map-based translation that occurred during this process, which is equivalent to counterclockwise rotation. The color version of this figure is available only in the electronic edition.

with interpretations based on well and high-resolution seismic reflection data by the previous authors for the fault onshore and in the outer harbor area, where it overlies the Wilmington anticline (Stephenson *et al.*, 1995; McNeilan *et al.*, 1996; Goodman *et al.*, 2015).

We next extend our kinematic model in 3D to explore implications for the geometry and map trace of the Palos Verdes fault (Figs. 7, 8; Fig. S1). This model suggests that the growth of the Wilmington anticline can rotate the map trace of the PVFZ counterclockwise by 10°–25°, which is consistent with the present-day trace (Fig. 8). In addition, the counterclockwise rotation produced by our kinematic model is localized at the geographic location where the map trace of the fault bends (Stephenson *et al.*, 1995; McNeilan *et al.*, 1996; Goodman *et al.*, 2015).

We found that the imposed initial dip of the PVFZ does not have first-order control on the resulting cross-sectional and map pattern orientation of the PVFZ. Although shallower initial dips for the PVFZ result in more degrees of rotation and steepening, all initial fault dips result in rotations of the PVFZ to steep (>70°) or vertical in the shallow subsurface. This is consistent with interpretations of steep fault strands in the near-surface onshore portion of the PVFZ. Moreover, we suggest that onshore high-angle strands may represent synthetic branching strands from a progressively rotating PVFZ during this deformation process, as suggested by the relative age and slip rates on each splay demonstrating a prolonged rotation history. Older faults are located to the southwestern portion of the fault splay package, whereas, younger, more recently formed splays are to the northeast (Stephenson *et al.*, 1995; Goodman *et al.*, 2015). This is analogous to the previous studies in thrust systems, in which fanning splays located along prominent bends in underlying structures are commonly associated with the folded fault remaining active while being folded (Dahlstrom, 1970; Morley, 1988).

In map view, shallower initial fault configurations lead to greater degrees of counterclockwise rotation; however, the overall range in rotation is small relative to the overall effect. The 20° bend onshore is consistent with a moderately dipping PVFZ, including the down-dip geometry documented by Brankman and Shaw (2009) for the San Pedro Shelf portion of the PVFZ (preferred dip: 45°) and the blind reverse fault interpreted by Goodman *et al.* (2015). Adjustments to the orientation of the inclined shear vector, consistent with the ranges defined previously (N1°W–N30°E) also contributed in a minor way to the overall effect. More easterly strikes led to more overall rotation, however, only impacting the final trace by ~1°–2°.

Finally, we suggest that our kinematic modeling results also prohibit the initial geometry of the PVFZ from being strictly a vertical fault. If the folding vector field defined here were resolved on an initial vertical fault, it would rotate the upper reaches of the fault into an eastward-dipping orientation, which is inconsistent with all the previous investigations of the geometry of the PVFZ onshore and with the significant west-side-up vertical offset observed across the PVFZ onshore (e.g., Fig. 4) (Ward and Valensise, 1994; Stephenson *et al.*, 1995; McNeilan *et al.*, 1996; Goodman *et al.*, 2015).

In summary, we suggest that interaction of the Palos Verdes fault and Wilmington anticline is a viable mechanism to explain the origin of the restraining bend in the fault that forms the Palos Verdes Peninsula (Nardin and Henyey, 1978; Bryant, 1987; Ward and Valensise, 1994). Specifically, this model suggests that the Palos Verdes fault at shallow levels steepens its dip beneath the Palos Verdes Peninsula where its map trace rotates from N40°W to N65°W (Wright, 1991; Kelsch, 1996). Both the change of fault dip and trend forms a restraining bend in the Palos Verdes fault, which enhances the vertical component of fault slip driving uplift of the Palos Verdes Peninsula. This restraining bend is thus interpreted as the northward continuation of the Palos Verdes fault in San Pedro Bay, where the faults dips to the southwest and exhibits oblique, reverse right-lateral motion (Kelsch, 1996; Rigor, 2003; Bohannon *et al.*, 2004; Fisher *et al.*, 2004a; Brankman and Shaw, 2009). Shallow splays along the entire trace of the fault partition oblique slip at depth into components of strike- and dip-slip motion that vary based on their orientations. We suggest that this 3D model of the Palos Verdes fault reconciles the shallow subsurface observations and interpretations made onshore and in the outer harbor (Stephenson *et al.*, 1995; McNeilan *et al.*, 1996; Goodman *et al.*, 2015) with constraints on the deeper architecture of the offshore fault in San Pedro Bay (Brankman and Shaw, 2009). Paleomagnetic data on the Palos Verdes Peninsula is limited; however, Seyum *et al.* (2008) document 10.2° ± 9° of clockwise, vertical axis rotation on Miocene sedimentary rocks located on the Peninsula since the Miocene. This is a relatively minor amount of rotation contrasts with the large amount of rotation recorded in the Western Transverse ranges to the north and further offshore to the west within Santa Catalina Island (Luyendyk *et al.*, 1980; Seyum *et al.*, 2008; Stewart, 2019). A portion of this disagreement could be accounted for by the counterclockwise rotation of the Palos Verdes fault by the underlying WBT.

Santa Monica Bay segment

Previous work. North of the Palos Verdes Peninsula, debate persists over the extent, geometry, and evidence for recent activity on the PVFZ. One reason is due to the difficulty in imaging the fault zone where uplifted areas of the Santa Monica Bay expose Miocene strata at the seafloor and do not preserve the effect of active faulting on a young sedimentary package (i.e., the Pliocene to Quaternary section has been eroded away) (Junger and Wagner, 1977). Repeated episodes of subaerial exposure and erosion during the Pleistocene have reduced preservation of Pliocene and Quaternary sediments along the fault trace and thus limit possible evidence of recent faulting (Fisher *et al.*, 2003). Because of the absence of clear

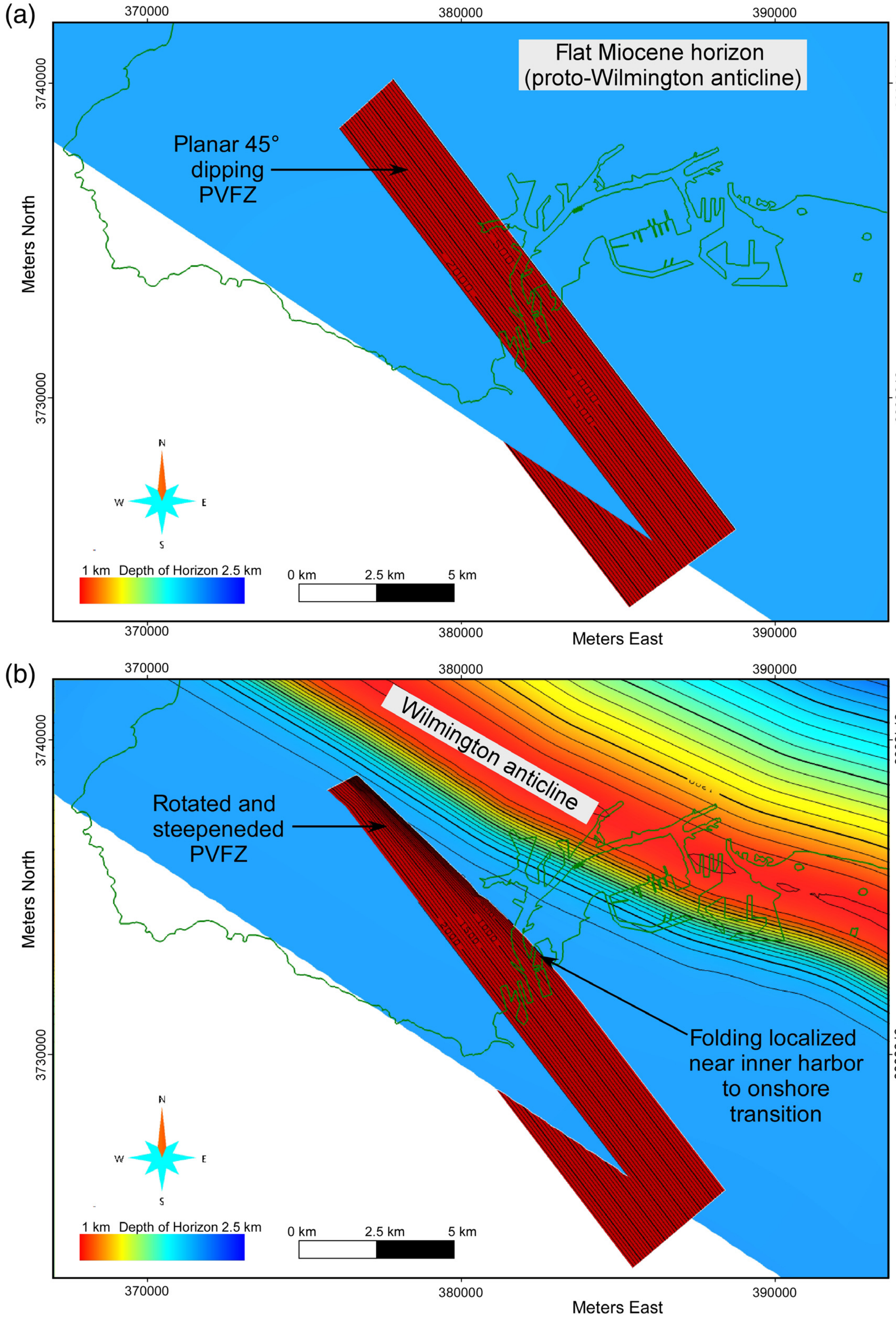

Figure 7. The 3D model demonstrating the warping of the PVFZ by the Wilmington anticline. (a) An initial planar PVFZ is modeled across the offshore–onshore transition. The late Miocene strata (blue surface) are deposited flat before the reactivation of the WBT (Wolfe *et al.*, 2019) (b) Final result of our 3D kinematic modeling of the growth of the Wilmington anticline, which folds the PVFZ and rotates it counterclockwise (see Fig. S1 for description of modeling procedure). In the shallow subsurface, the PVFZ is much steeper onshore than offshore, where it is further away from the Wilmington anticline. Map axes coordinates are shown in NAD27/UTM Zone 11N (m). The color version of this figure is available only in the electronic edition.

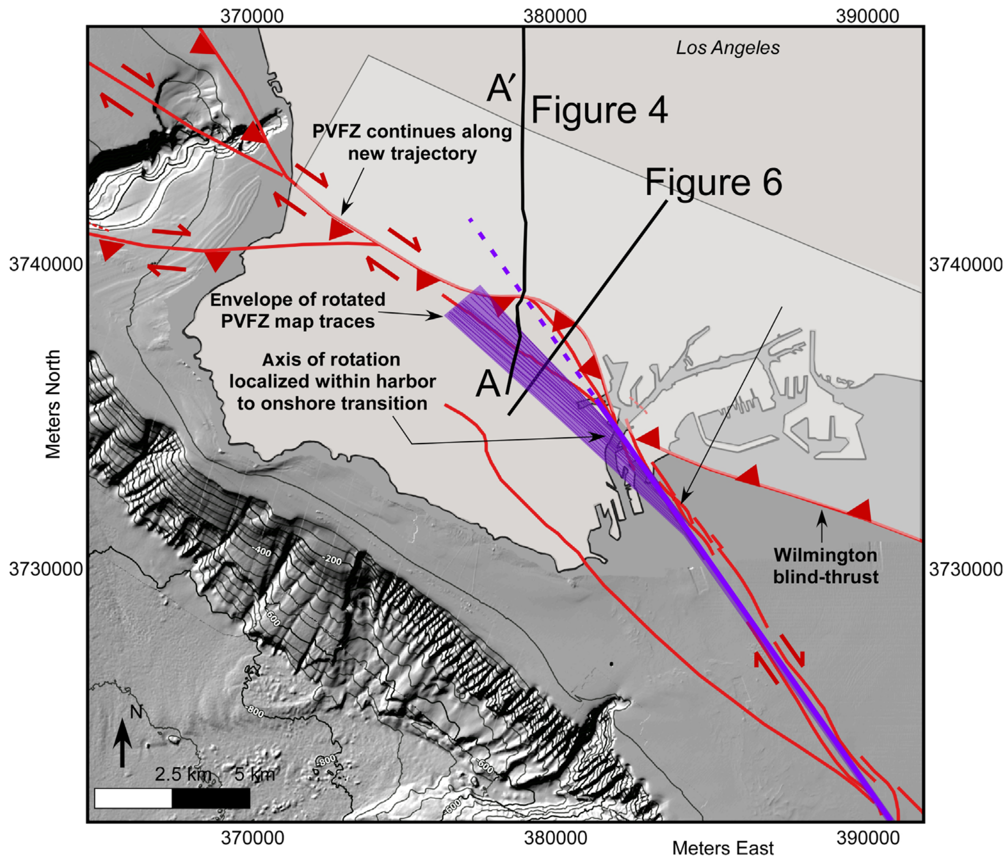

Figure 8. Map view of the kinematic modeling results. Results of 3D kinematic modeling demonstrate the map-based rotation of the PVFZ that occurred while it was warped by the underlying Wilmington anticline. The purple dashed line represents the initial trace of the PVFZ. The transparent purple envelope encompassing the thin purple lines represents the range of outcomes from our 3D kinematic modeling procedure. The thin purple lines are the position of the PVFZ in the individual trial runs. The bathymetry is from Gardner and Dartnell (2002). The surface trace of the WBT north of the intersection with the PVFZ is not shown for simplicity. As shown in Figure 4, the WBT continues northward beneath the Torrance anticline and is located in the footwall of the PVFZ. Map axes coordinates are shown in NAD27/UTM Zone 11N (m). The color version of this figure is available only in the electronic edition.

deformation signatures in young sediments, some researchers suggest that activity on the Santa Monica Bay segment is primarily pre-Quaternary, or that the fault zone does not extend far north of the Palos Verdes Peninsula (Junger and Wagner, 1977; Fisher *et al.*, 2003; Bohannon *et al.*, 2004). Others have interpreted strands of the fault zone truncating beneath a pre-Quaternary unconformity (Hogan *et al.*, 2008).

One model suggests that the PVFZ merges with and loses displacement onto the RCFZ, which is interpreted as a south-dipping reverse fault extending west-southwest across the Santa Monica shelf with minor deformation distributed across the shelf north of the Redondo Canyon (Nardin and Henyey, 1978; Fisher *et al.*, 1987; Wright, 1991; Fig. 1). In this model, horsetail strands splay westward from the PVFZ and have reverse separation (Fig. 9), consistent with accommodating motion on the PVFZ (Nardin and Henyey, 1978).

Other researchers have documented a broad zone of active deformation across the Santa Monica shelf representing the northward continuation of the PVFZ. This is consistent with a broad zone of distributed seismicity observed in the Santa Monica Bay, including numerous earthquakes (Fig. 2) with reverse-fault focal mechanisms (e.g., Malibu earthquakes 1979 and 1989 of M_w 5) that are too far south to be attributed the east–west-trending Santa Monica–Anacapa–Dume (SMAD) oblique, reverse sinistral fault system (Hauksson and Saldivar, 1989; Hauksson, 1990). Seafloor lineaments, disrupted seafloor ravines, and a seafloor slump at the head of the Redondo Canyon have been interpreted as evidence for the fault's recent activity (Hogan *et al.*, 2007). In the northern reaches of the Santa Monica Bay, several studies have documented active contractional folding above southwest-dipping fault splays that offset late Pleistocene-to-Holocene sediments and may cut the seafloor (Larson, 2000; Sorlien *et al.*, 2006; Hogan *et al.*, 2007). Some authors extend the PVFZ to an intersection with the SMAD fault system (Fig. 9a), in which it is assumed to terminate or be truncated by these faults that define the southern margin of the Western Transverse ranges (Jennings, 1994; Sorlien *et al.*, 2006).

3D fault architecture. To investigate the nature of the PVFZ in the Santa Monica Bay, we interpreted a dense grid of high-resolution, marine-seismic reflection data (Fig. 9a; see Data and Resources for processing information on seismic surveys). We georeferenced these into the geologic modeling software SKUA-GOCAD by Paradigm and depth converted them using the Southern California Earthquake Center (SCEC) Community Velocity Model (Shaw *et al.*, 2015; Fig. 9).

These data suggest that multiple splays of the PVFZ are well imaged, produce mappable basement offset, and can be traced from onshore Palos Verdes Peninsula northwestward across the Santa Monica Bay for 20 km at an azimuth of 280°–350°. Overall, the PVFZ separates two distinct structural domains. Northeast of the PVFZ is a thick sequence of nearly flat lying, undeformed, continuous reflectors corresponding to late

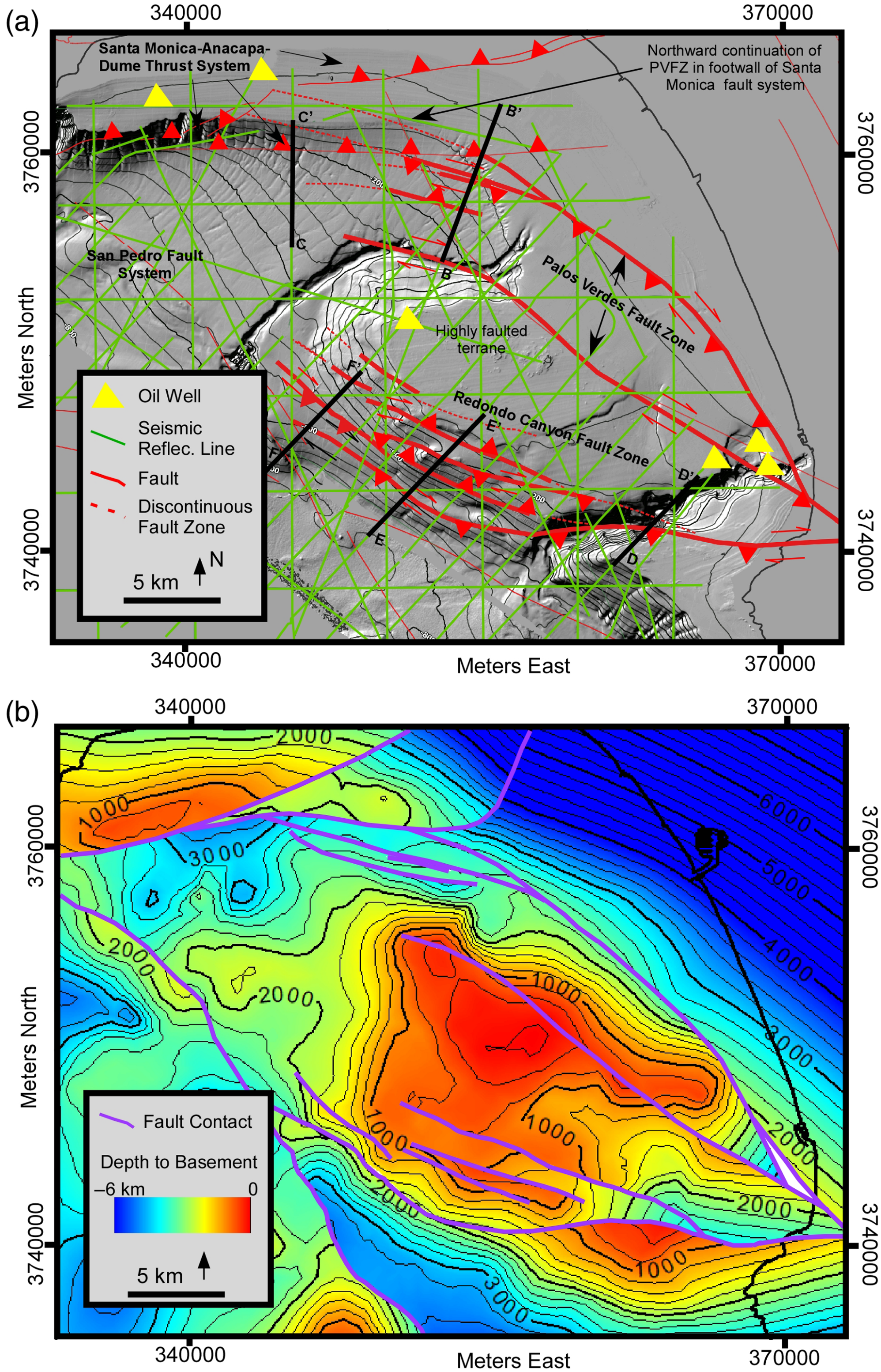

Figure 9. Santa Monica Bay segment of the PVFZ. (a) Bathymetric map of the Santa Monica Bay segment, including the RCFZ and other active faults in the region. Bathymetry from Gardner and Dartnell (2002). The grid of seismic reflection data used in this study is shown as thin green lines. Wells with documented penetrations of schist (i.e., these are likely at or near the basement contact) in the Santa Monica Bay are shown as yellow triangles. Locations for Figures 10, 12, and 13 shown as black bold lines. (b) The top of the Catalina Schist gridded interpretation with fault cuts identified by purple lines and significant basement offset. Faults in inset (b) are labeled in (a). Map axes coordinates are shown in NAD27/UTM Zone 11N (m). The color version of this figure is available only in the electronic edition.

Miocene to Pliocene sediments, whereas, southwest of the PVFZ, the strata are uplifted above the basement-cored and highly faulted offshore shelf projection Palos Verdes anticlinorium.

Figure 10 shows a seismic reflection line across the main strand of the Santa Monica Bay segment of the PVFZ. Here, the PVFZ has a moderate dip at depth and is composed of two faults that contains multiple splays in their hanging walls (Fig. 10; faults A and B). The dip of the fault zone (~40°–60°) is indicated by the cutoff geometries imaged on the Catalina Schist Basement horizon. The down-dip portion of this fault zone is similar to the geometry proposed by Sorlien *et al.* (2006). Up-dip of the main fault ramps, Sorlien *et al.* (2006) interprets these faults to extend to the seafloor. Our data suggest that this may be the case; however, all or most of the slip on some faults may also be consumed by folding in front of a blind fault tip. In this case, the seafloor manifestation of active deformation would be in the form of folding rather than faulting. In addition, the Miocene strata interpreted in the hanging wall of the main fault ramps thicken eastward toward the faults. These units are much thicker than their correlative units east of the fault zone in its footwall. Toward the southwest, these strata are interpreted to onlap onto a basement high, similar to the observations made by Sorlien *et al.* (2006). These observations are consistent with Miocene strata filling a graben above a normal fault that was later reactivated as a

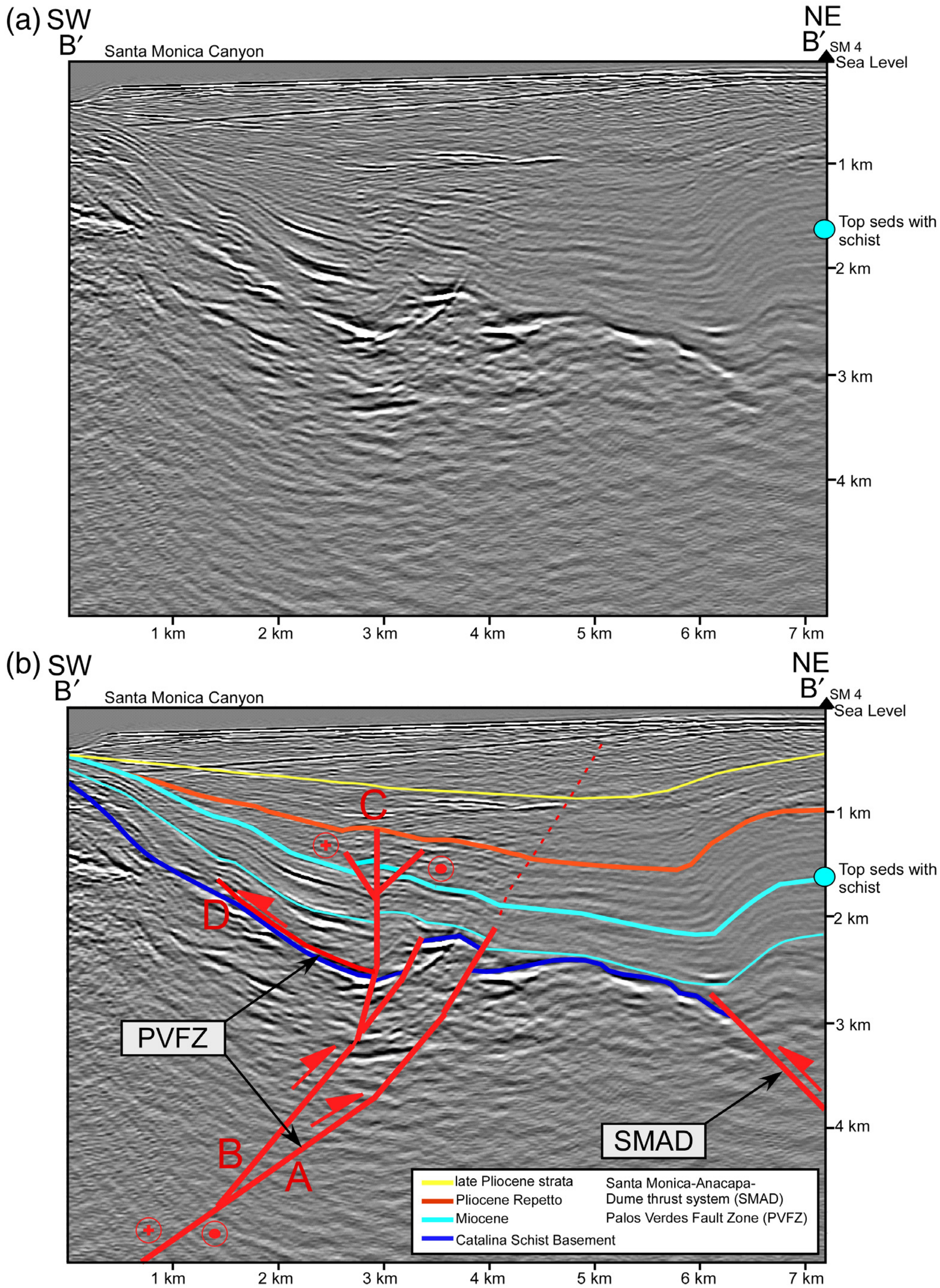

Figure 10. Structural architecture of the Santa Monica Bay segment of the PVFZ. (a) Uninterpreted and (b) interpreted seismic reflection line across the Santa Monica Bay segment. Southern extent of the Santa Monica–Anacapa–Dume (SMAD) fault system shown on the right side of seismic section. The location of the seismic reflection line is shown in Figure 9a. Slip indicators are provided, as well as labels for faults mentioned in the 3D Fault Architecture section. The color version of this figure is available only in the electronic edition.

transpressional structure during the Pliocene. This deformation history is similar to that proposed for the San Pedro Bay segment (Brankman and Shaw, 2009; Fig. 11).

The fault B of the PVFZ in Santa Monica Bay has an additional strike-slip fault in its hanging wall (Fig. 10; fault C). Adjacent to the strike-slip splay, a local pop-up structure is present. This configuration is evidence that the PVFZ accommodates both strike-slip and dip-slip motion, which has been suggested for the broader PVFZ both onshore (Goodman *et al.*, 2015) and within the San Pedro Bay (Brankman and Shaw, 2009), as well as a distributed pattern of strike-, reverse-, and oblique-slip focal mechanisms in the Santa Monica Bay (Hauksson *et al.*, 2012; Yang *et al.*, 2012). Fault C also has an east-dipping reverse-fault splay (Fig. 10; fault D) in its hanging wall that appears to be located along the contact of the Catalina Schist crystalline basement and the overlying late Miocene deep-water marine shales of Mohnian age. The geometry of the overlying fold indicates that this fault likely only accommodated a minor amount of slip of the entire system and is consistent with a similar feature was documented by Brankman and Shaw (2009) for the San Pedro Bay segment of the PVFZ (Fig. 11).

Within both Figures 10 and 12, it is evident that the reverse displacement observable on the Catalina Schist basement is much less than the 1.8 km of west-side-up vertical separation that is observed onshore at the location of the Palos Verdes Peninsula. In some cases (e.g., Fig. 10; fault B), the basement still resolves net normal offset. In other cases, the basement has reverse offset of <500 m (e.g., Fig. 10; fault A). This is consistent with the previous interpretations (e.g., Nardin and Henyey, 1978), which suggest that Pliocene to recent displacement on the fault zone decreases northward into the Santa Monica Bay.

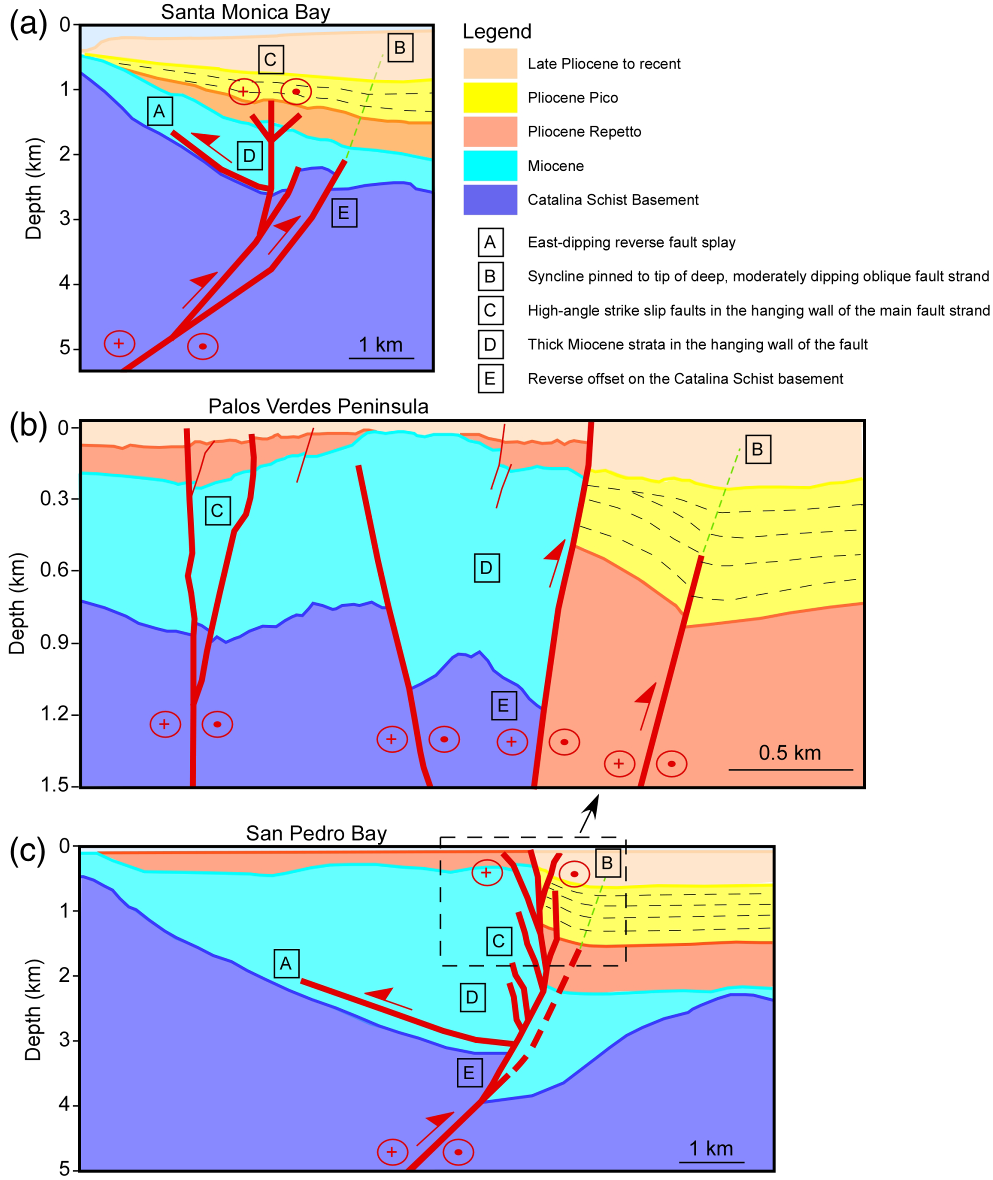

Figure 11. Simplified cross sections across the PVFZ. (a) Santa Monica Bay segment. (b) San Pedro Bay segment onshore at the location of the Palos Verdes Peninsula, after Goodman *et al.* (2015). This section describes the deformation pattern in the shallow subsurface, and the relative location of this inset within the upper portions of the PVFZ is shown as a dashed box in inset (c). (c) San Pedro Bay segment offshore, after Brankman and Shaw (2009). Each segment of the PVFZ shares a similar deformation pattern, as described by the elements A–E. The locations of cross sections (a–c) are shown in Figure 2. The color version of this figure is available only in the electronic edition.

In the northern Santa Monica Bay, the PVFZ takes a 25° counterclockwise rotation and aligns more northwesterly, where it strikes close to the SMAD north-dipping reverse-fault system (Fig. 9a). Figure 11 shows how the zone of deformation surrounding the tip of the Santa Monica Bay segment of the PVFZ is similar to that described in Figure 10. These similarities include: (1) stratigraphic cutoffs on the Catalina Schist basement that suggest that the main Santa Monica Bay segment dips moderately to the southwest; (2) onlap of Miocene strata westward onto a basement high in the hanging wall of the fault ramp; and (3) a north-vergent forelimb of a fault-propagation fold that is located above the fault tip (Fig. 11). The fold is located in the footwall of the SMAD thrust system. Because of the amount of displacement and relief of the latter, which was significant enough to uplift the Santa Monica Mountains, as well as the relative position of the PVFZ in its footwall, we agree with the previous interpretations that the PVFZ fault truncates into this thrust system (Fig. 12) (Jennings, 1994; Sorlien *et al.*, 2006).

The RCFZ. Our analysis of marine seismic reflection data in the Santa Monica Bay suggests that the PVFZ continues offshore north of the Palos Verdes Peninsula beneath the bay. Thus, the PVFZ is a broadly continuous feature, but the Santa Monica Bay segment may accommodate significantly less displacement than the adjoining San Pedro Bay segment. This suggests that displacement on the main strand of the Palos Verdes fault may transfer to numerous northwest-oriented branches within a broad damage zone that represents the northern extent of the PVFZ (Nardin and Henyey, 1978). The RCFZ has been recognized as one of the main candidates for accommodating a component of this displacement (Nardin and Henyey, 1978; Bohannon *et al.*, 2004).

In concordance with the previous work by Nardin and Henyey (1978) and Bohannon *et al.* (2004), our analysis suggests that the RCFZ branches from the PVFZ within the northern reaches of the PVFZ (Fig. 9). The RCFZ causes a significant change in basement elevation, while juxtaposing a Miocene interval on the Palos Verdes shelf south of the fault with a thick section of Quaternary strata to the north of the fault zone

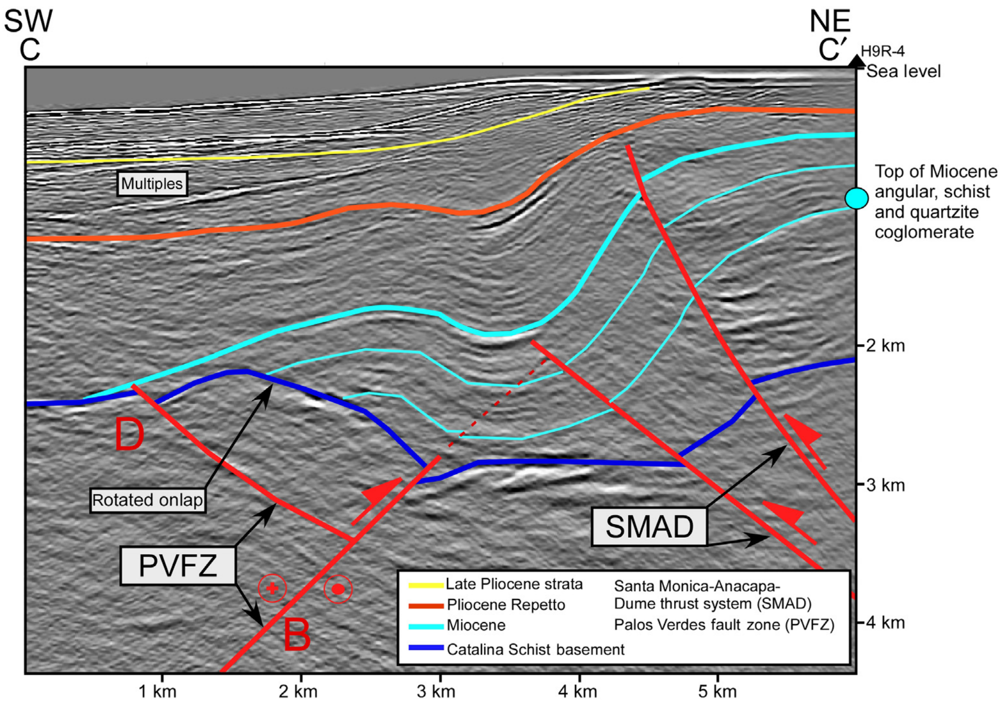

Figure 12. Interpreted seismic reflection line in the Santa Monica Bay near the SMAD. Here, the fault is interpreted to truncate into the footwall of the SMAD. The deformation pattern in this location is similar to the deformation pattern interpreted in Figure 10, demonstrating the consistency of the style of deformation along strike of the PVFZ in the Santa Monica Bay. The location of the seismic reflection line is shown in Figure 9a. The color version of this figure is available only in the electronic edition.

(Emery, 1960; Yerkes *et al.*, 1967; Nardin and Henyey, 1978) (Fig. 13a). The overall geometry of the fault zone is oriented east–west to northwest–southeast and dips to the south. The fault cuts the seafloor and Holocene deposits on the shelf south of the head of Redondo Canyon, as well as the southern canyon wall (Fig. 13a; Nardin and Henyey, 1978; Bohannon *et al.*, 2004).

The RCFZ splits into several branches in an area of faulted anticlines on the lower slope west of Redondo Canyon (Fig. 13b, c). Many of these faults dip steeply and contain thickened sections of Miocene strata directly in their hanging walls. In addition, some faults resolve reverse offset in the shallow subsurface, whereas the basement has normal offset (Fig. 13b). In some places, strata onlap onto basement highs and are rotated in the hanging walls of contractional features (Fig. 13b). These observations are all consistent with faults that initiated as normal faults during the late Miocene and reactivated as oblique reverse faults during the postearly Pliocene (Crouch and Suppe, 1993; Brankman and Shaw, 2009; Wolfe *et al.*, 2019).

Some of the RCFZ splays are blind and deform Holocene deposits in their overlying folds (Fig. 13). In present-day deep water settings, these produce emergent seafloor scarps with varying relief (e.g., Fig. 13b,c). In shallower waters, such as just south of the Redondo Canyon, anticlinal crests uplifted above blind strands of the RCFZ were likely eroded during the Last Glacial Maximum or the previous glacial periods when the sea levels were significantly lower than the present day (e.g., Fig. 13a; Clark *et al.*, 2014). Other splays appear to extend to the seafloor based on offset shallow stratigraphy, including a major splay that crops out at base of the canyon.

Although the main strand of the RCFZ is dipping to the south at the Redondo Canyon, additional northeast dipping splays can be correlated between seismic reflection lines. These fault splays produce continuous uplifts of Miocene and Pliocene strata that can be correlated to outcrops on the San Pedro Shelf, bounding the western edge of the offshore Palos Verdes shelf projection anticlinorium (Bohannon *et al.*, 2004).

At the northern extent of the RCFZ, the fault merges or truncates into the San Pedro basin fault. This region is characterized by a broad, west-dipping, less-deformed Santa Monica shelf slope that is dissected by a few minor blind faults and associated uplifts (Figs. 9; 13c). This deformation pattern contrasts with the character in the regions to the south where the fault appears to be more active. Thus, we interpret that slip dies out to the north on this fault system, as it is possibly transferred to the San Pedro basin fault. Figure 13c shows the northernmost east-vergent fault-propagation folds above a west-dipping blind reverse fault marks the northern extent of the RCFZ.

Based on these observations, we conclude that the RCFZ and associated splays to the north in Santa Monica Bay represent a broad damage zone associated with the northern termination of the PVFZ. This is consistent with the general interpretations of Nardin and Henyey (1978) and Bohannon *et al.* (2004) and demonstrated by our 3D fault model (Fig. 14). Such damage zones are common geologic features interpreted to form due to stress concentrations at fault tips and linking zones (e.g., Chester and Logan, 1986; Cox and Scholz, 1988; Cowie and Scholz, 1992; Gupta and Scholz, 2000), and/or to accommodate displacement variations along faults (e.g., Vermilye and Scholz, 1998; Kim *et al.*, 2000). At the brittle terminations of strike-slip faults, these commonly involve synthetic branching of faults with the same sense of slip as the master fault (Chinnery, 1966a, 1966b; Tapponnier and Molnar, 1979; Kim *et al.*, 2001, 2003, 2004; Chen *et al.*, 2002).

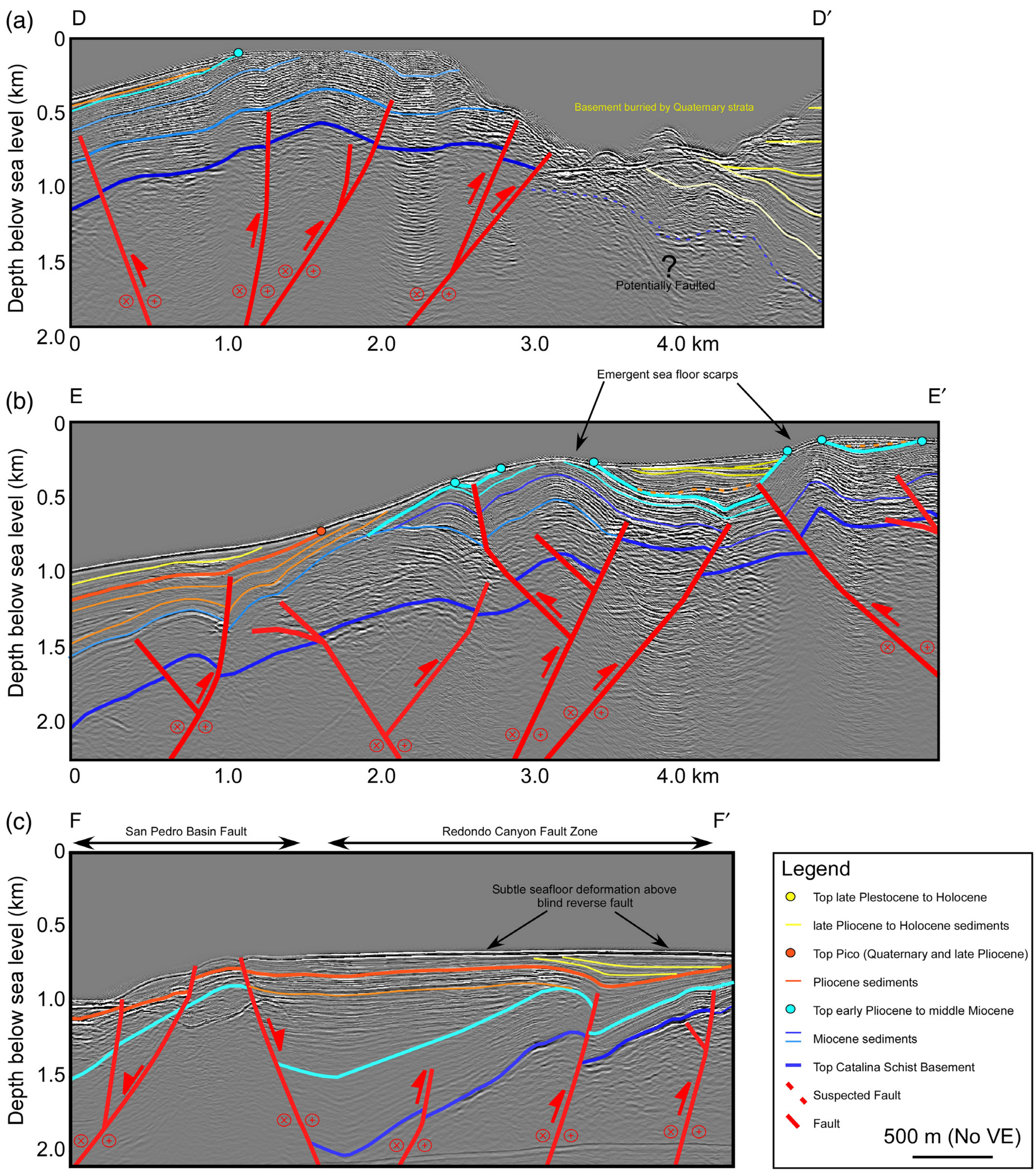

Figure 13. Seismic reflection data showing the architecture of the RCFZ, which is composed of numerous high-angle reverse faults that are likely reactivated Miocene normal faults. (a) Canyon section, (b) central slope section, and (c) northern section document the changing architecture of the fault system along strike. Some faults still preserve net normal displacement despite evidence for recent reverse displacement due to the phase of late Miocene faulting. Stratigraphy at the seafloor are tied to geologic maps of Bohannon *et al.* (2004). The locations of these seismic reflection lines are shown in Figure 9a. The color version of this figure is available only in the electronic edition.

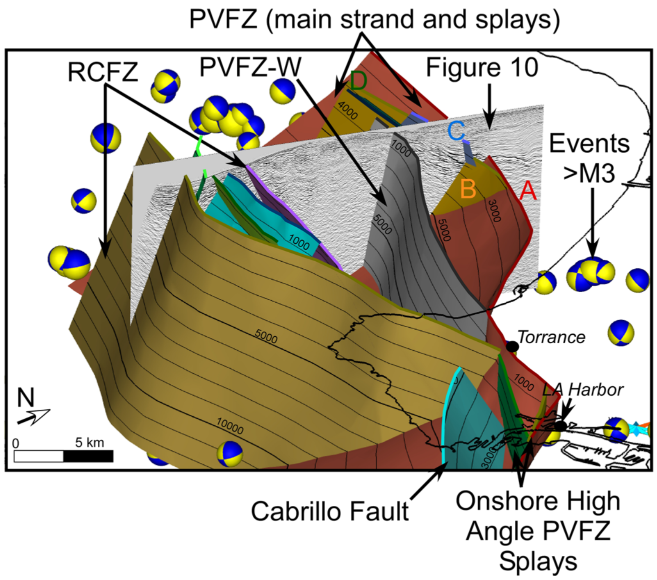

Figure 14. The 3D model of the faults within the Santa Monica Bay. Analysis of marine seismic reflection data reveals the presence of multiple active fault splays within the PVFZ and RCFZ offshore within the Santa Monica Bay. Labels are placed near faults mentioned in the 3D Fault Architecture section. Earthquake focal mechanisms from Yang *et al.* (2012) and Hauksson *et al.* (2012). All numbered contours are in kilometer units. Surface traces of faults shown with bold colored traces. The color version of this figure is available only in the electronic edition.

Multiple segments of the RCFZ show direct evidence of the recent activity. This is consistent with observations of scattered small earthquakes near trace of the RCFZ (Ziony, 1985; Hauksson and Saldivar, 1989; Yang *et al.*, 2012; Yang and Hauksson, 2013; Ross *et al.*, 2019). These events include the 8 May 2021 M_w 3.7 earthquake, which occurred 5 km off the coast of Hermosa Beach and was felt onshore. The focal mechanism for the event is a pure dip-slip solution above a moderately westward-dipping fault plane (40°–50°) (see Data and Resources).

Lasuen Knoll segment

The Lasuen Knoll segment is the southernmost portion of the PVFZ (Fig. 2). The fault segment extends from the base of the San Pedro slope along the western edge of the San Gabriel Canyon at a water depth of 250–600 m and continues offshore for 40 km, where it bounds the eastern margin of the Lasuen Knoll uplift (Marlow *et al.*, 2000; Normark *et al.*, 2001; Gardner and Dartnell, 2002; Fisher *et al.*, 2004b). The previous studies have noted that the Lasuen Knoll segment of the fault zone is clearly expressed by seafloor scarps and subtle along-strike bends identified in multibeam bathymetric data (Marlow *et al.*, 2000; Brankman and Shaw, 2009; Brothers *et al.*, 2015).

Seismic reflection profiles collected across this segment image a near-vertical zone of disrupted reflectors with discontinuous, anastomosing, and subvertical fault splays. The sense of vertical offset is east-side-up on the principal trace of the fault system, which has been interpreted to dip moderately eastward at an angle of 40°–75° (preferred dip: 70°) (Brankman and Shaw, 2009). Alternatively, other authors (Brothers *et al.*, 2015) have interpreted the Lasuen Knoll segment as a near-vertical fault zone or a fault that dips at a low angle locally near the Knoll but steeply dipping elsewhere (Fisher *et al.*, 2004b). Vertical relief increases to the south along this segment, ultimately resulting in the emergence of the basement block forming the Lasuen Knoll to the east of the mapped fault trace. The southern boundary of the Lasuen Knoll segment is interpreted south of the Lasuen Knoll basement block uplift, where the uplift plunges southward and vertical displacement decreases. Further south, some researchers propose that the fault zone continues southeast as the Coronado Bank fault zone with alternating regions of transpressional pop-up structures and broad transtensional sags (Legg, 1991; Legg and Kennedy, 1991; Legg *et al.*, 2007). However, published hazard assessments (e.g., Field *et al.*, 2013) and CFMs (Plesch *et al.*, 2007) consider the Coronado Bank fault zone separate from the PVFZ.

In contrast to the San Pedro and Santa Monica Bay segments, the Lasuen Knoll segment shows no evidence of a Miocene rift history (Brankman and Shaw, 2009). This may explain why the fault has a geometry that is clearly distinct from that of the San Pedro and Santa Monica Bay segments. Dextral oblique reverse motion initiated on the principal trace of the Lasuen Knoll segment during the middle Pliocene. Recent estimates of strike-slip rates are 1.3–2.8 mm/yr, as determined by measuring offsets along multiple tectonogeomorphic features (Brothers *et al.*, 2015; Table 1).

DISCUSSION

A new comprehensive model of the PVFZ

We combine our analysis of faults within Santa Monica Bay and the onshore Peninsula with results from the prior studies that have documented the fault geometry in San Pedro Bay (Bryant and Raub, 1986; Kelsch, 1996; McNeilan *et al.*, 1996; Marlow *et al.*, 2000; Bohannon *et al.*, 2004; Fisher *et al.*, 2004b; Brankman and Shaw, 2009) to build a new comprehensive 3D model for the Palos Verdes fault (Fig. 15). This model differs from that used in current seismic hazard assessments, which generally represent the fault as a simple, vertical surface and do not include the full extent or detailed fault zone geometry described herein and by others (McNeilan *et al.*, 1996; Brankman and Shaw, 2009; Brothers *et al.*, 2015; Goodman *et al.*, 2015). Our new model illustrates that the PVFZ is a long, continuous structure with multiple segments that exhibit complex geometries and kinematics.

For the Lasuen Knoll segment, we incorporate the preferred dip interpreted by Brankman and Shaw (2009) (70° to the east) and the fault trace mapped by Brothers *et al.* (2015). For San Pedro Bay segment, we use the fault geometry prescribed by

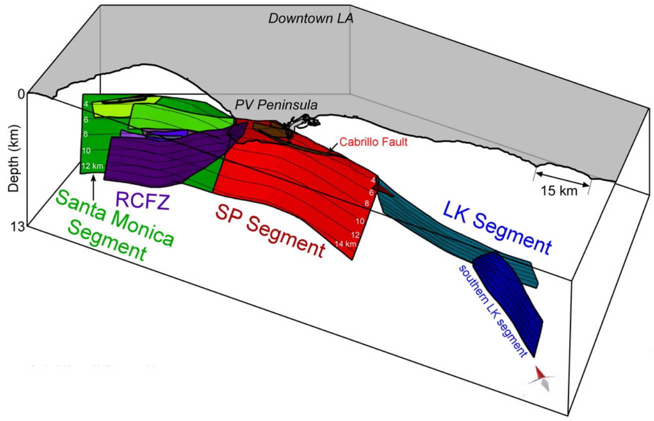

Figure 15. New comprehensive model of the PVFZ and 3D perspective view of the faults considered for hazard analysis. Faults are shown to intersect with the base of the seismogenic crust (Nazareth and Hauksson, 2004). The southern Lasuen Knoll segment is consistent with southern California community fault model (CFM) representations (Plesch *et al.*, 2007). The color version of this figure is available only in the electronic edition.

Brankman and Shaw (2009), including the preferred dip of 45° to the west. We also include the Cabrillo fault, which has previously been considered a splay of the PVFZ and shows evidence for recent activity on the Palos Verdes Peninsula (Bryant and Raub, 1986; Figs. 3; 15). Onshore, we also model the downdip portions of the Palos Verdes fault with a 45° dip, which is consistent with interpretations of a moderately dipping steep blind reverse fault interpreted in high-resolution seismic reflection data onshore (Goodman *et al.*, 2015). Near the surface, the fault steepens, and we include multiple high-angle hanging-wall splays previously mapped by Goodman *et al.* (2015). In the Santa Monica Bay, we build upon the work of Nardin and Henyey (1978), Bohannon *et al.* (2004), and Sorlien *et al.* (2006) by including the full 3D architecture of multiple strands of the fault system as well as its entire northward extent. We model a moderately dipping fault ramp (~45°–50°) and include the high-angle hanging-wall splay interpreted by Sorlien *et al.* (2006), as well as numerous splays interpreted in seismic reflection data within this study. This high-angle hanging-wall splay is the main Santa Monica Bay segment of the PVFZ in the current representation of the CFM for southern California (Sorlien *et al.*, 2006; Plesch *et al.*, 2007; Fig. 15).

Finally, our new model incorporates the full 3D architecture of the RCFZ, including numerous south- and north-dipping moderate-to-high-angle faults. All segments of the PVFZ are interpreted above the base of the seismogenic crust (Nazareth and Hauksson, 2004; Fig. 15; Table S2).

Rupture scenarios and seismic hazard

Our 3D fault models allow us to calculate the area of the PVFZ and its independent segments to estimate the maximum magnitudes of earthquakes they may generate. Because of the major changes in fault geometry and kinematics across these major segments, segment boundaries may limit the extent of earthquake ruptures (Brankman and Shaw, 2009). Alternatively, the broad continuity of the PVFZ suggests that earthquake rupture may be able to breach these geometric segment boundaries. Thus, we consider both individual and multisegment ruptures of the PVFZ. All 3D fault models extend downward to the base of the seismogenic crust defined by Nazareth and Hauksson (2004), consistent with the approach of the CFM (Plesch *et al.*, 2007). We do not explicitly include uncertainty in the depth to the base of the seismogenic crust in our calculation of fault areas. Rather, we consider our fault areas to be minima for each of the segments, with the possibility that ruptures extending deeper in the crust would increase fault areas and thus potential earthquake magnitudes. This methodology follows that of the previous studies for estimating deterministic seismic hazard assessment from 3D fault models (Brankman and Shaw, 2009; Field and Page, 2011; Hubbard *et al.*, 2014; Morell *et al.*, 2020; Felix *et al.*, 2021), such as that for the WBT (Wolfe *et al.*, 2019).

For this assessment, we use the published empirical relations between rupture area, moment magnitude, and average displacement for all the fault types (Hanks and Bakun, 2002, 2008; Biasi and Weldon, 2006; Table S1). To relate average displacement from an earthquake on the PVFZ to a recurrence interval, we consider the previous estimates and define a preferred slip rate for the entire PVFZ that encompasses the entire range of the published values inclusive of their reported uncertainties (Table 1). We calculated an average displacement from empirical relations between average displacement and magnitude (Table S1). Next, we calculated the recurrence interval by dividing the average displacement in a scenario rupture by the upper and lower slip rate bounds defined in Table 1. We consider average displacement for rupture scenarios rather than maxima or minima, because displacement patterns in strike- and oblique-slip earthquake are often highly complex, with significant variations in displacement caused by details of local fault geometry mapped at the surface (e.g., Sieh *et al.*, 1993). Given that we cannot resolve these local details in fault geometry at seismogenic depths, we consider it appropriate to use average displacements consistent with the approach of the previous studies (Brankman and Shaw, 2009; Hubbard *et al.*, 2014; Wolfe *et al.*, 2019).

Our choice of a single, broad slip-rate range to define the entire PVFZ is motivated by the observation that the most recent estimates for slip rate on the PVFZ are closely aligned across the Lasuen Knoll and San Pedro Bay segments (Brankman and Shaw, 2009; Brothers *et al.*, 2015; Goodman *et al.*, 2015). In the Santa Monica Bay, no constraint exists on the recent slip rate of the fault, but the overall consistency of the fault geometry across the San Pedro and Santa Monica Bay segments motivates our approach to extend the San Pedro slip rate into the Santa Monica Bay. We acknowledge, however,

TABLE 2
Deterministic Seismic Hazard Scenarios for the Palos Verdes Fault Zone

Rupture Scenarios	Rupture Area (km^2)	Magnitude (M_w)*	Recurrence Interval (yr)*	Magnitude (M_w)†	Recurrence Interval (yr)†
Individual segments					
Lasuen Knoll (LK)	977	7.1	608 (191–1025)	7.2–7.4	601 (134–1067)
San Pedro Bay (SP)	910	7.0	586 (184–988)	7.1–7.3	582 (128–1035)
Santa Monica Bay (SMB)	949	7.0	599 (188–1010)	7.1–7.3	593 (132–1054)
Redondo Canyon fault zone (RCFZ)	716	6.9	519 (163–875)	7.0–7.3	523 (111–934)
Combined ruptures					
SMB + RCFZ	1665	7.4	797 (250–1343)	7.4–7.5	763 (184–1342)
LK + SP + SMB	2835	7.7	1044 (328–1761)	7.6–7.7	969 (252–1686)
LK + SP + RCFZ	2602	7.6	1000 (314–1685)	7.6–7.7	932 (240–1625)
LK + SP + SMB + RCFZ	3551	7.8	1171 (368–1974)	7.7–7.8	1072 (288–1857)

Rupture areas derived from 3D fault models. All models are assumed to rupture to the base of the seismogenic crust defined by Nazareth and Hauksson (2004) and listed in Table S2. Magnitude and recurrence interval estimates are based on empirical relationships listed in Table S1.
*Empirical relationships based on regressions for all fault types from Hanks and Bakun (2002, 2008) and Biasi and Weldon (2006).
†Empirical relationships based on regressions for strike-slip and reverse faults from Thingbaijam *et al.* (2017). See Table S3 for full results using these regressions.

the Santa Monica Bay segment could be slipping at a slower rate if the RCFZ or other northwest-oriented splays consume most or all of the recent displacement that would otherwise occur on the Santa Monica Bay segment. Presently, the slip rate on the RCFZ is poorly constrained but is inferred to be similar to the vertical uplift rate for the PVFZ (Treiman, 1998).

Considering the fault areas in our 3D model (Table S2), we define a number of potential rupture scenarios in Table 2. Ruptures on the Lasuen Knoll, San Pedro Bay, and Santa Monica Bay segments of the fault could generate M_w 7.1, 7.0, and 7.0 earthquakes, respectively. Linkages along strike would enable larger multisegment earthquakes. If all sections ruptured together, they could produce an M_w 7.8 earthquake. Ruptures along the entire PVFZ would occur less frequently, and would be controlled by slip rates and recurrence intervals on these faults.

Our choice to use the published regression relationships between fault area and earthquake magnitude for all the fault types was based on the complex, oblique-slip nature of the Palos Verdes fault. Alternatively, recent studies (e.g., Mai and Beroza, 2000; Blaser *et al.*, 2010) suggest that earthquake scaling relationships should be calculated with respect to faulting type. To date, regression relationships between fault size and earthquake magnitude do not exist explicitly for oblique-slip events like that expected on the PVFZ (Thingbaijam *et al.*, 2017). However, Thingbaijam *et al.* (2017) showed that for three recent oblique-slip events, fault size, and moment magnitude plotted within the range of expected values derived from scaling laws of strike-slip and reverse-faulting events. Using the Thingbaijam *et al.* (2017) scaling relationship between fault area and moment magnitude (Table S1), the Lasuen Knoll, San Pedro Bay, and Santa Monica Bay segments of the fault could each generate M_w 7.1–7.4 earthquakes, and a full rupture of the fault would generate an M_w 7.7–7.8 earthquake. These single and multisegment event magnitudes are similar or slightly greater than our previously discussed estimates using Hanks and Bakun (2002, 2008) and Biasi and Weldon (2006). The single and multisegment rupture scenarios based on the Thingbaijam *et al.* (2017) are provided in Table S3, including both magnitude and recurrence interval estimates.

Collectively, these scenarios provide higher seismic hazard calculations than previously reported by current models that include a vertical fault without significant splays and not extending for the full trace of the PVFZ (Plesch *et al.*, 2007, 2020). Our new representations extend the fault further along strike and include additional segments that act together as a complex fault system to accommodate slip on the PVFZ. In addition, our model includes a moderately dipping PVFZ at depth yielding a larger potential rupture area. The dip of the fault with a component of reverse displacement also compounds the seismic hazard, as future large earthquake would be expected to uplift the seafloor and could produce local tsunamis.

CONCLUSIONS

The PVFZ extends for more than 110 km offshore from the northern part of the Santa Monica Bay, onshore below the Palos Verdes Peninsula, and offshore beneath the San Pedro Bay, the San Pedro shelf, and deep water zone near Lasuen Knoll. The fault is composed of three segments with several major splays, which we describe in a new comprehensive, structural model.

Onshore, the PVFZ has a prominent restraining bend that uplifts the Palos Verdes Peninsula. Our kinematic models demonstrate how the growth of the Wilmington anticline in the footwall of the Palos Verdes fault is a plausible explanation for the origin of this feature. In the Santa Monica Bay, the PVFZ continues northward until it truncates into the footwall of the SMAD fault system. Many aspects of the fault zone, including the fault geometry and presence of high-angle hanging-wall splays are similar to that observed within southern segments of the fault zone. Uniquely, the Santa Monica Bay segment of the PVFZ contains numerous synthetic branching splays within a broad damage zone within the Santa Monica Bay, including the RCFZ, which shows evidence for recent activity and may accommodate a portion of the slip on the PVFZ.

We combine these insights to develop a comprehensive 3D model of the PVFZ. Our fault model yields an updated assessment of the seismic hazard posed by the PVFZ. Single-segment ruptures could produce M_w 7.1–7.4 earthquakes with a recurrence interval of 580–610 yr, whereas multisegment ruptures would enable larger earthquakes (e.g., M_w 7.4–7.8) with a recurrence interval of 760–1170 yr. Given the fast slip rate, the PVFZ represents one of the largest deterministic seismic hazards in the broader metropolitan Los Angeles region.

DATA AND RESOURCES

Seismicity data used in this article were downloaded from the Waveform Relocated Earthquake Catalogue for Southern California (Hauksson *et al.*, 2012) and the Quake Template Matching (QTM) Seismicity Catalog: A template-matching catalog for Southern California (Ross *et al.*, 2019). Southern California Earthquake Center (SCEC) Data can be downloaded from https://scedc.caltech.edu/ (last accessed November 2021). Some figures were drafted using QGIS software, Anaconda Jupyter Python coding interphase, ObsPy Python Toolbox for seismology and seismological observatories, Emerson E&P SKUA-GOCAD software, and Petroleum Experts MOVE software. Fault traces and regional fault surfaces were downloaded from SCEC Community Fault Model (CFM) and U.S. Geological Survey (USGS) Quaternary Fault Fold Database found at www.scec.org/research/cfm and www.usgs.gov, respectively (both last accessed May 2021). The 2D seismic reflection data came from the National Archive of Marine Seismic Surveys (O-1-99-SC, B-06-85-SC, A-1-98-SC, and W-5-82-SC), which can be found at https://walrus.wr.usgs.gov/namss (last accessed May 2021). The W-5-82-SC survey is a 2D multichannel, migrated, and stacked seismic reflection survey. The B-06-85-SC survey is a 2D multichannel stacked seismic reflection survey. The O-1-99-SC survey is a 2D multichannel, migrated, and stacked seismic reflection survey. The A-1-98-SC survey is a multichannel, migrated, and stacked seismic reflection survey. Additional processing information can be found for these two surveys at https://pubs.usgs.gov/of/2005/1084 (last accessed May 2022). Some well data came from the California Energy Management Division, which can be accessed at https://maps.conservation.ca.gov/doggr/ (last accessed May 2021). The supplemental material contains the following data and illustrations: (1) empirical relationships used for hazard calculations within the main body of the article, (2) estimates for depth of rupture based on the thickness of the seismogenic crust determined from our 3D fault model, (3) deterministic seismic hazard calculations using Thingbaijam *et al.* (2017) regressions, and (4) a description of the 3D kinematic modeling workflow.

DECLARATION OF COMPETING INTERESTS

The authors declare that there are no conflicts of interest recorded.

ACKNOWLEDGMENTS

Seismic reflection data were made available by PacSeis, Texaco, Inc., Chevron, Inc., and the U.S. Geological Survey (USGS) through the National Archive of Marine Seismic Surveys. Discussions with Jessica Don, Robert Welch, Kristen Chiama, Josimar Alves da Silva, and Izabella Sabharwal de Bessenyey inspired analysis conducted during this study. The authors are also thankful for reviews by Francesca Ghisetti and an anonymous reviewer, as well as guidance from Nicola Litchfield. Their thoughtful commentary helped to improve the article. The authors also wish to acknowledge generous donations of software used in this study. These include Emerson E&P SKUA-GOCAD for 3D visualization, interpretation, and fault modeling, Landmark Graphics for availability to seismic and well data, and Petroleum Experts for access to MOVE Structural Geology Modeling Software, which underpinned our kinematic modeling analysis and 3D visualization of fault surfaces.

REFERENCES

Allmendinger, R. W. (1998). Inverse and forward numerical modeling of trishear fault-propagation folds, *Tectonics* **17,** no. 4, 640–656.

Allmendinger, R. W., T. Zapata, R. Manceda, and F. Dzelalija (2004). Trishear kinematic modeling of structures, with examples from the Neuqun Basin, Argentina, in *Thrust Tectonics and Petroleum Systems*, K. R. McClay (Editor), Vol. 82, American Association of Petroleum Geologists Memoir, Tulsa, Oklahoma, 356–371.

Argus, D. F., M. B. Heflin, A. Donnellan, F. H. Webb, D. Dong, K. J. Hurst, D. C. Jefferson, G. A. Lyzenga, M. M. Watkins, and J. F. Zumberge (1999). Shortening and thickening of metropolitan Los Angeles measured and inferred by using geodesy, *Geology* **27,** no. 8, 703–706.

Atwater, T., and J. Stock (1998). Pacific-North America plate tectonics of the Neogene Southwestern United States: An update, *Int. Geol. Rev.* **40,** no. 5, 375–402.

Biasi, G. P., and R. J. Weldon (2006). Estimating surface rupture length and magnitude of paleoearthquakes from point measurements of rupture displacement, *Bull. Seismol. Soc. Am.* **96,** no. 5, 1612–1623.

Bjorklund, T., and K. Burke (2002). Four-dimensional analysis of the inversion of a half-graben to form the Whittier fold–fault system of the Los Angeles basin, *J. Struct. Geol.* **24,** no. 9, 1369–1387.

Blaser, L., F. Krüger, M. Ohrnberger, and F. Scherbaum (2010). Scaling relations of earthquake source parameter estimates with special focus on subduction environment, *Bull. Seismol. Soc. Am.* **100,** no. 6, 2914–2926.

Bohannon, R. G., and J. V Gardner (2004). Submarine landslides of San Pedro Escarpment, southwest of Long Beach, California, *Mar. Geol.* **203,** no. 3, 261–268.

Bohannon, R. G., and E. Geist (1998). Upper crustal structure and Neogene tectonic development of the California continental borderland, *Geol. Soc. Am. Bull.* **110,** no. 6, 779–800.

Bohannon, R. G., J. V. Gardner, and R. W. Sliter (2004). Holocene to Pliocene tectonic evolution of the region offshore of the Los Angeles urban corridor, southern California, *Tectonics* **23,** no. 1, TC1016, doi: 10.1029/2003TC001504.

Brankman, C. M., and J. H. Shaw (2009). Structural geometry and slip of the Palos Verdes Fault, Southern California: Implications for earthquake hazards, *Bull. Seismol. Soc. Am.* **99,** no. 3, 1730–1745.

Brothers, D. S., J. E. Conrad, K. L. Maier, C. K. Paull, M. McGann, and D. W. Caress (2015). The Palos Verdes Fault offshore Southern California: Late Pleistocene to present tectonic geomorphology, seascape evolution, and slip rate estimate based on AUV and ROV surveys, *J. Geophys. Res.* **120,** no. 7, 4734–4758.

Bryant, M. E. (1987). Emergent marine terraces and quaternary tectonics: Palos Verdes Peninsula, California, in *Geology of the Palos Verdes Peninsula and San Pedro Bay*, P. J. Fischer (Editor), Pacific Section SEPM, Santa Barbara, California, 63–78.

Bryant, M. E., and M. L. Raub (1986). The Cabrillo fault—A structural problem, Palos Verdes Peninsula in *Geology and Landslides of Palos Verdes Hills, California: Guidebook*, E. J. Baldwin (Editor), National Association of Geology Teachers, Northfield, Minnesota, 64–68.

Buddin, T. S., S. J. Kane, G. D. Williams, and S. S. Egan (1997). A sensitivity analysis of 3-dimensional restoration techniques using vertical and inclined shear constructions, *Tectonophysics* **269,** no. 1, 33–50.

Chen, Y., S. Gilder, N. Halim, J. P. Cogné, and V. Courtillot (2002). New paleomagnetic constraints on central Asian kinematics: Displacement along the Altyn Tagh fault and rotation of the Qaidam Basin, *Tectonics* **21,** no. 5, 1–6.

Chenghua, O., W. Chen, and Z. Ma (2015). Quantitative identification and analysis of sub-seismic extensional structure system: Technique schemes and processes, *J. Geophys. Eng.* **12,** no. 3, 502–514.

Chester, F. M., and J. M. Logan (1986). Implications for mechanical properties of brittle faults from observations of the Punchbowl fault zone, California, *Pure Appl. Geophys.* **124,** no. 1, 79–106.

Chinnery, M. A. (1966a). Secondary faulting: I. Geological aspects, *Can. J. Earth Sci.* **3,** no. 2, 163–174.

Chinnery, M. A. (1966b). Secondary faulting: II. Geological aspects, *Can. J. Earth Sci.* **3,** no. 2, 175–190.

Clark, J., J. X. Mitrovica, and J. Alder (2014). Coastal paleogeography of the California–Oregon–Washington and Bering Sea continental shelves during the latest Pleistocene and Holocene: Implications for the archaeological record, *J. Archaeol. Sci.* **52,** 12–23.

Connors, C. D., A. N. Hughes, and S. M. Ball (2021). Forward kinematic modeling of fault-bend folding, *J. Struct. Geol.* **143,** doi: 10.1016/j.jsg.2020.104252.

Cooke, M. L., and S. T. Marshall (2006). Fault slip rates from three-dimensional models of the Los Angeles metropolitan area, California, *Geophys. Res. Lett.* **33,** no. 21, L21313, doi: 10.1029/2006GL027850.

Corredor, F., J. H. Shaw, and F. Bilotti (2005). Structural styles in the deep-water fold and thrust belts of the Niger Delta, *Am. Assoc. Pet. Geol. Bull.* **89,** no. 6, 753–780.

Cowie, P. A., and C. H. Scholz (1992). Physical explanation for the displacement-length relationship of faults using a post-yield fracture mechanics model, *J. Struct. Geol.* **14,** no. 10, 1133–1148.

Cox, S. J. D., and C. H. Scholz (1988). On the formation and growth of faults: An experimental study, *J. Struct. Geol.* **10,** no. 4, 413–430.

Crouch, J. K., and J. Suppe (1993). Late Cenozoic tectonic evolution of the Los Angeles basin and inner California borderland: A model for core complex-like crustal extension, *GSA Bull.* **105,** no. 11, 1415–1434.

Cunningham, W. D., and P. Mann (2007). Tectonics of strike-slip restraining and releasing bends, *Geol. Soc. Lond. Spec. Publ.* **290,** no. 1, 1–12.

Dahlstrom, C. D. A. (1970). Structural geology in the eastern margin of the Canadian Rocky Mountains, *Bull. Can. Pet. Geol.* **18,** no. 3, 332–406.

Darrow, A., and P. J. Fischer (1983). Activity and earthquake potential of the Palos Verdes fault, *U.S. Geol. Surv. Technical Rept.*, Reston, Virginia, 90 pp.

Davis, T. L., J. Namson, and R. F. Yerkes (1989). A cross section of the Los Angeles Area: Seismically active fold and thrust belt, The 1987 Whittier Narrows earthquake, and earthquake hazard, *J. Geophys. Res.* **94,** no. B7, 9644–9664.

Dolan, J. F., K. Sieh, T. K. Rockwell, R. S. Yeats, J. Shaw, J. Suppe, G. J. Huftile, and E. M. Gath (1995). Prospects for larger or more frequent earthquakes in the Los Angeles metropolitan region, *Science* **267,** no. 5195, 199–205.

Douilly, R., H. Aochi, E. Calais, and A. M. Freed (2015). Three-dimensional dynamic rupture simulations across interacting faults: The Mw7. 0, 2010, Haiti earthquake, *J. Geophys. Res.* **120,** no. 2, 1108–1128.

Elliott, A. J., M. E. Oskin, J. Liu-Zeng, and Y. Shao (2015). Rupture termination at restraining bends: The last great earthquake on the Altyn Tagh fault, *Geophys. Res. Lett.* **42,** no. 7, 2164–2170.

Emery, K. O. (1960). *The Sea Off Southern California, A Modern Habitat of Petroleum*, University of Southern California, Los Angeles, California, 1–366.

Erslev, E. A. (1991). Trishear fault-propagation folding, *Geology* **19,** no. 6, 617–620.

Felix, R. P., J. A. Hubbard, K. Bradley, K. Lythgoe, L. Li, and A. Switzer (2021). Tsunami hazard in Lombok & Bali, Indonesia, due to the Flores back-arc thrust, *Nat. Hazards Earth Sys. Sci.* Discuss, preprint, in review, doi: 10.5194/nhess-2021-343.

Field, E. H. (2000). Accounting for site effects in probabilistic seismic hazard analyses of Southern California: Overview of the SCEC Phase III report, *Bull. Seismol. Soc. Am.* **90**, no. 6B, S1–S31.

Field, E. H., and M. T. Page (2011). Estimating earthquake-rupture rates on a fault or fault system, *Bull. Seismol. Soc. Am.* **101,** no. 1, 79–92.

Field, E. H., G. P. Biasi, P. Bird, T. E. Dawson, K. R. Felzer, D. D. Jackson, K. M. Johnson, T. H. Jordan, C. Madden, A. J. Michael, *et al.* (2013). Uniform California earthquake rupture forecast, version 3 (UCERF3)—The time-independent model, *U.S. Geol. Surv. Open-File Rept. 2013-1165, Calif. Geol. Surv. Spec. Rep. 228, South. Calif. Earthq. Cent. Publ. 1792*, doi: 10.3133/ofr20131165.

Fisher, M. A., W. R. Normark, R. G. Bohannon, R. W. Sliter, and A. J. Calvert (2003). Geology of the continental margin beneath Santa Monica Bay, southern California, from seismic-reflection data, *Bull. Seismol. Soc. Am.* **93,** no. 5, 1955–1983.

Fisher, M. A., W. R. Normark, V. E. Langenheim, A. J. Calvert, and R. Sliter (1987). The Palos Verdes Fault Zone: Onshore to offshore, in *Geology of the Palos Verdes Peninsula and San Pedro Bay*, P. J. Fischer (Editor), Society for Sedimentary Geology, Los Angeles, California, 91–133.

Fisher, M. A., W. R. Normark, V. E. Langenheim, A. J. Calvert, and R. W. Sliter (2004a). Marine geology and earthquake hazards of the San Pedro shelf region, Southern California, *U.S. Geol. Surv. Profess. Pap. No. 1687*, 1–39.

Fisher, M. A., W. R. Normark, V. E. Langenheim, A. J. Calvert, and R. Sliter (2004b). The offshore Palos Verdes fault zone near San Pedro, Southern California, *Bull. Seismol. Soc. Am.* **94,** no. 2, 1–25.

Freeman, S. T., P. D. Guptill, T. A. Demerre, and D. L. Schug (1985). Late Quaternary activity along the onshore portion of the Palos Verdes fault zone, *Final Technical Report to the U.S. Geological Survey*, Contract No.14-08-0001-21304, scale 1:37,000, 83 pp.

Gardner, J. V, and P. Dartnell (2002). Multibeam mapping of the Los Angeles, California margin, *U.S. Geol. Surv. Open-File Rept. 2002-162*, doi: 10.3133/ofr02162.

Goodman, J. T., D. A. Ostenaa, P. J. Hogan, D. R. O'Connell, and J. P. Turner (2015). Strain partitioning along the onshore Palos Verdes Fault Zone: New constraints on the geometry, distribution and kinematics of Quaternary deformation, *Seismol. Res. Lett.* **86,** 734.

Greene, H. G., and M. P. Kennedy (Editors) (1987). *Geology of the Inner Southern California Continental Margin*, Resources Agency, State of California, Dept. of Conservation, Sacramento, California.

Griffiths, P., S. Jones, N. Salter, F. Schaefer, R. Osfield, and H. Reiser (2002). A new technique for 3-D flexural-slip restoration, *J. Struct. Geol.* **24,** no. 4, 773–782.

Groshong, R. H., Jr. (1990). Unique determination of normal fault shape from hanging-wall bed geometry in detached half grabens, *Eclogae Geol. Helv.* **83,** no. 3, 455–471.

Gupta, A., and C. H. Scholz (2000). A model of normal fault interaction based on observations and theory, *J. Struct. Geol.* **22,** no. 7, 865–879.

Guzofski, C. A., J. P. Mueller, J. H. Shaw, P. Muron, D. A. Medwedeff, F. Bilotti, and C. Rivero (2009). Insights into the mechanisms of fault-related folding provided by volumetric structural restorations using spatially varying mechanical constraints, *Am. Assoc. Pet. Geol. Bull.* **93,** no. 4, 479–502.

Hamblin, W. K. (1965). Origin of "reverse drag" on the downthrown side of normal faults, *Geol. Soc. Am. Bull.* **76,** no. 10, 1145–1164.

Hamling, I. J., S. Hreinsdóttir, K. Clark, J. Elliott, C. Liang, E. Fielding, N. Litchfield, P. Villamor, L. Wallace, and T. J. Wright (2017). Complex multifault rupture during the 2016 Mw 7.8 Kaikōura earthquake, New Zealand, *Science* **356,** no. 6334, doi: 10.1126/science.aam7194.

Hanks, T. C., and W. H. Bakun (2002). A bilinear source-scaling model for M—log A observations of continental earthquakes, *Bull. Seismol. Soc. Am.* **92,** 1841–1846.

Hanks, T. C., and W. H. Bakun (2008). M-logA Observations for Recent Large Earthquakes, *Bull. Seismol. Soc. Am.* **98,** no. 1, 490–494.

Hardy, S., and E. Finch (2007). Mechanical stratigraphy and the transition from trishear to kink-band fault-propagation fold forms above blind basement thrust faults: A discrete-element study, *Mar. Pet. Geol.* **24,** no. 2, 75–90.

Hauksson, E. (1990). Earthquakes, faulting, and stress in the Los Angeles Basin, *J. Geophys. Res.* **95,** no. B10, 15,365–15,394.

Hauksson, E. (2000). Crustal structure and seismicity distribution adjacent to the Pacific and North America plate boundary in southern California, *J. Geophys. Res.* **105,** no. B6, 13,875–13,903.

Hauksson, E., and G. Saldivar (1989). Seismicity and active compressional tectonics in the Santa Monica Bay, *South. Calif. J. Geophys. Res.* **94,** 9591–9606.

Hauksson, E., and G. V. Saldivar (1986). The 1930 Santa Monica and the 1979 Malibu, California, earthquakes, *Bull. Seismol. Soc. Am.* **76,** no. 6, 1542–1559.

Hauksson, E., W. Yang, and P. M. Shearer (2012). Waveform relocated earthquake catalog for Southern California (1981 to June 2011): Short Note, *Bull. Seismol. Soc. Am.* **102,** no. 5, 2239–2244.

Hogan, P. J., A. Broughton, K. Smith, M. Legg, T. McNeilan, and R. R. Male (2007). New kinematic model for the Palos Verdes and San Pedro Basin fault zones in Santa Monica Bay, offshore southern California, *Am. Assoc. Pet. Geol. Bull.* 91 pp.

Hogan, P. J., A. Lane, J. Hooper, A. Broughton, and B. Romans (2008). Geohazard challenges of the Woodside OceanWay LNG development, Offshore Southern California, *Offshore Technology Conference*, Houston, Texas.

Hubbard, J., J. H. Shaw, J. F. Dolan, T. L. Pratt, L. J. McAuliffe, and T. K. Rockwell (2014). Structure and seismic hazard of the Ventura Avenue anticline and Ventura fault, California: Prospect for large, multisegment ruptures in the Western Transverse Ranges, *Bull. Seismol. Soc. Am.* **104,** no. 3, 1070–1087.

Jennings, C. W. (1994). Fault activity map of California and adjacent areas, with locations of recent volcanic eruptions, California Division of Mines and Geology Geologic Data Map 6, 2 pls., scale 1:750,000, 92 p.

Jones, L., K. Aki, D. Boone, M. Celebi, A. Donnellan, J. Hall, R. Harris, E. Hauksson, T. Heaton, S. Hough, *et al.* (1994). The magnitude 6.7 Northridge, California, earthquake of 17 January 1994, *Science* **266,** no. 5184, 389–397.

Junger, A., and H. C. Wagner (1977). Geology of the Santa Monica and San Pedro basins, California Continental Borderland, *U.S. Geol. Surv.*, 9 maps scale 2400, doi: 10.3133/mf820.

Kelsch, K. D. (1996). Three-dimensional tectonostratigraphic development of the Los Angeles Basin as viewed through the Beta 3D seismic survey oil field, *Master's Thesis*, California State University Northridge, Department of Geological Sciences, 183 pp.

Kim, Y.-S., J. R. Andrews, and D. J. Sanderson (2000). Damage zones around strike-slip fault systems and strike-slip fault evolution, Crackington Haven, southwest England, *Geosci. J.* **4,** no. 2, 53–72.

Kim, Y.-S., J. R. Andrews, and D. J. Sanderson (2001). Secondary faults and segment linkage in strike-slip fault systems at Rame Head, southern Cornwall, *Geosci. South-West Engl.* **10,** no. 2, 123–133.

Kim, Y.-S., D. C. P. Peacock, and D. J. Sanderson (2003). Mesoscale strike-slip faults and damage zones at Marsalforn, Gozo Island, Malta, *J. Struct. Geol.* **25,** no. 5, 793–812.

Kim, Y.-S., D. C. P. Peacock, and D. J. Sanderson (2004). Fault damage zones, *J. Struct. Geol.* **26,** no. 3, 503–517.

Larson, A. A. (2000). Defining the fault that caused the 1979 and 1989 Malibu Earthquakes (M 5.0) in Santa Monica Bay, California, *Sr. Thesis*, Harvard University, Department of Earth and Planetary Sciences, 65 pp.

Legg, M. R. (1991). Developments in understanding the tectonic evolution of the California Continental Borderland, in *From Shoreline to Abyss: Contributions in Marine Geology in Honor of Francis Parker Shepard*, R. H. Osborne (Editor), Special Publications of SEPM, Tulsa, Oklahoma, 291–312.

Legg, M. R., and M. P. Kennedy (1991). Oblique divergence and convergence in the California Continental Borderland, in *Environmental Perils of the San Diego Region*, P. L. Abbott and W. J. Elliot (Editors), San Diego Association of Geologists Guidebook, San Diego, California, 1–16.

Legg, M. R., C. Goldfinger, M. J. Kamerling, J. D. Chaytor, and D. E. Einstein (2007). Morphology, structure and evolution of California Continental Borderland restraining bends, *Geol. Soc. Lond. Spec. Publ.* **290,** no. 1, 143–168.

Lingrey, S., and O. Vidal-Royo (2015). Evaluating the quality of bed length and area balance in 2D structural restorations, *Interpretation* **3,** no. 4, SAA133–SAA160.

Litchfield, N. J., P. Villamor, R. J. Van Dissen, A. Nicol, P. M. Barnes, D. J. A. Barrell, J. R. Pettinga, R. M. Langridge, T. A. Little, and J. J. Mountjoy (2018). Surface rupture of multiple crustal faults in the 2016 Mw 7.8 Kaikōura, New Zealand, Earthquake, *Bull. Seismol. Soc. Am.* **108,** no. 3B, 1496–1520.

Lozos, J. C., D. D. Oglesby, J. N. Brune, and K. B. Olsen (2012). Small intermediate fault segments can either aid or hinder rupture propagation at stepovers, *Geophys. Res. Lett.* **39,** no. 18, L18305, doi: 10.1029/2012GL053005.

Luyendyk, B. P. (1991). A model for Neogene crustal rotations, transtension, and transpression in southern California, *Geol. Soc. Am. Bull.* **103,** no. 11, 1528–1536.

Luyendyk, B. P., M. J. Kamerling, and R. Terres (1980). Geometric model for Neogene crustal rotations in southern California, *Geol. Soc. Am Bull.* **91,** no. 4, 211–217.

Mai, P. M., and G. C. Beroza (2000). Source scaling properties from finite-fault-rupture models, *Geol. Soc. Am. Bull.* **90,** no. 3, 604–615.

Marlow, M. S., J. V. Gardner, and W. R. Normark (2000). Using high-resolution multibeam bathymetry to identity seafloor surface rupture along the Palos Verdes fault complex in offshore Southern California, *Geology* **28,** no. 7, 587–590.

McNeilan, T., T. Rockwell, and G. Resnick (1996). Style and rate of Holocene slip, Palos Verdes Fault, Southern California, *J. Geophys. Res.* **101,** 8317–8334.

Meade, B. J., and B. H. Hager (2005). Block models of crustal motion in southern California constrained by GPS measurements, *J. Geophys. Res.* **110,** no. B3, doi: 10.1029/2004JB003209.

Mitra, S. (1990). Fault-propagation folds: Geometry, kinematic evolution, and hydrocarbon traps, *Am. Assoc. Pet. Geol. Bull.* **74,** no. 6, 921–945.

Morell, K. D., R. Styron, M. Stirling, J. Griffin, R. Archuleta, and T. Onur (2020). Seismic hazard analysis from geologic and geomorphic data: Current and future challenges, *Tectonics* **39,** e2018TC005365, doi: 10.1029/2018TC005365.

Morley, C. K. (1988). Out-of-sequence thrusts, *Tectonics* **7,** no. 3, 539–561.

Nardin, T. R., and T. L. Henyey (1978). Pliocene-Pleistocene diastrophism of Santa Monica and San Pedro Shelves, California Continental Borderland, *Am. Assoc. Pet. Geol. Bull.* **62,** no. 2, 247–272.

Nazareth, J. J., and E. Hauksson (2004). The seismogenic thickness of the southern California Crust, *Bull. Seismol. Soc. Am.* **94,** 940–960.

Nicholson, C., C. C. Sorlien, T. Atwater, J. C. Crowell, and B. P. Luyendyk (1994). Microplate capture, rotation of the western Transverse Ranges, and initiation of the San Andreas transform as a low-angle fault system, *Geology* **22,** no. 6, 491–495.

Normark, W. R., S. Baher, and R. W. Sliter (2001). Late Quaternary sedimentation and deformation in Santa Monica and Catalina basins, offshore Southern California, in *Geology and Tectonics of Santa Catalina Island and the California Continental Borderland, Field Trip Guidebook*, South Coast Geological Society, Orange County, California, Vol. 32, 291–317.

Novoa, E., J. Suppe, and J. H. Shaw (2000). Inclined-shear restoration of growth folds, *Am. Assoc. Pet. Geol. Bull.* **84,** no. 6, 787–804.

Olsen, K. B. (2000). Site amplification in the Los Angeles basin from three-dimensional modeling of ground motion, *Bull. Seismol. Soc. Am.* **90,** no. 6B, S77–S94.

Otott, G., D. Clarke, and T. Buikema (1996). Long beach unit 3-D survey, in *Old Oil Fields and New Life: A Visit to the Giants of the Los Angeles Basin*, D. Clarke, G. E. Otott, and C. C. Phillips (Editors), Division of Environmental Geosciences, American Association of Petroleum Geologists, Pacific Section, Bakersfield, California, 51–55.

Plesch, A., S. T. Marshall, C. Nicholson, J. H. Shaw, P. J. Maechling, and M. Su (2020). The Community Fault Model version 5.3 and new web-based tools, *SCEC Annual Meeting, Poster 184*, SCEC Contribution #10547, Palm Springs, California, September 2020.

Plesch, A., J. H. Shaw, C. Benson, W. A. Bryant, S. Carena, M. Cooke, J. Dolan, G. Fuis, E. Gath, L. Grant, *et al.* (2007). Community Fault Model (CFM) for Southern California, *Bull. Seismol. Soc. Am.* **97,** no. 6, 1793–1802.

Rigor, A. W. (2003). Structure and deformation of the Palos Verdes Fault in San Pedro Bay, California, *Master's Thesis*, San Diego State University, Department of Geological Sciences, 87 pp.

Ross, Z. E., D. T. Trugman, E. Hauksson, and P. M. Shearer (2019). Searching for hidden earthquakes in Southern California, *Science* **364,** no. 6442, 767–771.

Rouby, D., H. Xiao, and J. Suppe (2000). 3-D restoration of complexly folded and faulted surfaces using multiple unfolding mechanisms, *Am. Assoc. Pet. Geol. Bull.* **84,** no. 6, 805–829.

Schoellhamer, J. E., and A. O. Woodford (1951). The Floor of the Los Angeles Basin, Los Angeles, Orange and San Bernardino Counties, California, *U.S. Geol. Surv. Oil and Gas Inv. Map OM-117*, doi: 10.3133/om117.

Seyum, S., A. Oshiro, and N. Onderdonk (2008). Neogene tectonic rotation of the Palos Verdes Peninsula, *Geol. Soc. Am. Abstr. Progr.* **40,** no. 1, 53.

Shackleton, J. R., and M. L. Cooke (2007). Is plane strain a valid assumption in non-cylindrical fault-cored folds? *J. Struct. Geol.* **29,** no. 7, 1229–1240.

Shaw, J. H., and P. M. Shearer (1999). An elusive blind-thrust fault beneath metropolitan Los Angeles, *Science* **283,** no. 5407, 1516–1518.

Shaw, J. H., and J. Suppe (1996). Earthquake hazards of active blind-thrust faults under the central Los Angeles basin, California, *J. Geophys. Res.* **101,** 8623–8642.

Shaw, J. H., F. Bilotti, and P. A. Brennan (1999). Patterns of imbricate thrusting, *Bull. Geol. Soc. Am.* **111,** no. 8, 1140–1154.

Shaw, J. H., C. Connors, and J. Suppe (2005). *Seismic Interpretation of Contractional Fault-Related Folds*, Vol. 53, American Association of Petroleum Geologists, doi: 10.1306/St531003.

Shaw, J. H., E. Novoa, and C. D. Connors (2005). Structural controls on growth stratigraphy in contractional fault-related folds, in *Thrust Tectonics and Hydrocarbon Systems*, K. R. McClay (Editor), Vol. 82, AAPG Memoir, Tulsa, Oklahoma, 400–412.

Shaw, J. H., A. Plesch, C. Tape, M. P. Suess, T. H. Jordan, G. Ely, E. Hauksson, J. Tromp, T. Tanimoto, R. Graves, *et al.* (2015). Unified structural representation of the southern California crust and upper mantle, *Earth Planet. Sci. Lett.* **415,** 1–15.

Sibson, R. H. (1985). Stopping of earthquake ruptures at dilational fault jogs, *Nature* **316,** no. 6025, 248–251.

Sieh, K., L. Jones, E. Hauksson, K. Hudnut, D. Eberhart-Phillips, T. Heaton, S. Hough, K. Hutton, H. Kanamori, A. Lilje, *et al.* (1993). Near-field investigations of the Landers earthquake sequence, April to July 1992, *Science* **260,** no. 5105, 171–176.

Sorlien, C. C., M. J. Kamerling, L. Seeber, and K. G. Broderick (2006). Restraining segments and reactivation of the Santa Monica–Dume–Malibu Coast fault system, offshore Los Angeles, California, *J. Geophys. Res.* **111,** no. B11, doi: 10.1029/2005JB003632.

Sorlein, C. C., L. Seeber, K. G. Broderick, B. P. Luyendyk, M. A. Fischer, R. W. Sliter, and W. R. Normark (2013). The Palos Verdes anticlinorium along the Los Angeles, California coast: Implications for underlying thrust faulting, *Geochem. Geophys. Geosys.* **14,** 1866–1890.

Stephenson, W. J., T. Rockwell, J. Odum, and D. A. Okaya (1995). Seismic reflection and geomorphic characterization of the onshore Palos Verdes fault zone, Los Angeles, California, *Bull. Seismol. Soc. Am.* **85,** 943–950.

Stewart, R. A. (2019). Miocene rotation of Santa Catalina Island: Implications for the Southern California Continental Borderland, *Master's Thesis*, California State University, Department of Geological Sciences, Long Beach, California, 113 pp.

Suppe, J., and D. Medwedeff (1990). Geometry and kinematics of fault-propagation folding, *Eclogae Geol. Helv.* **83,** 409–454.

Suppe, J., G. T. Chou, and S. C. Hook (1992). Rates of folding and faulting determined from growth strata, in *Thrust Tectonics*, K. R. McClay (Editor), Springer Netherlands, Dordrecht, The Netherlands, 105–121, doi: 10.1007/978-94-011-3066-0_9.

Tapponnier, P., and P. Molnar (1979). Active faulting and Cenozoic tectonics of the Tien Shan, Mongolia, and Baykal regions, *J. Geophys. Res.* **84,** no. B7, 3425–3459.

Tchalenko, J. S. (1970). Similarities between shear zones of different magnitudes, *Geol. Soc. Am. Bull.* **81,** no. 6, 1625–1640.

Thingbaijam, K. K. S., P. M. Mai, and K. Goda (2017). New empirical earthquake source-scaling laws, *Bull. Seismol. Soc. Am.* **107,** no. 5, 2225–2246.

Treiman, J. A. (1998). Fault number 130, Redondo Canyon fault, Quatery Fault and Fold Database of the United States, *U.S. Geol. Surv. Website* available at https://earthquakes.usgs.gov/hazards/qfaults (last accessed May 2022).

U.S. Geological Survey and California Geological Survey (2006). Quaternary Fault and Fold Database of the United States, available at https://earthquakes.usgs.gov/hazards/qfaults (last accessed May 2022).

Vermilye, J. M., and C. H. Scholz (1998). The process zone: A microstructural view of fault growth, *J. Geophys. Res.* **103,** no. B6, 12,223–12,237.

Walls, C., T. Rockwell, K. Mueller, Y. Bock, S. Williams, J. Pfanner, J. Dolan, and P. Fang (1998). Escape tectonics in the Los Angeles metropolitan region and implications for seismic risk, *Nature* **394,** no. 6691, 356–360.

Ward, S. N., and G. Valensise (1994). The Palos Verdes terraces, California: Bathtub rings from a buried reverse fault, *J. Geophys. Res.* **99,** no. B3, 4485–4494.

Wei, S., E. Fielding, S. Leprince, A. Sladen, J. P. Avouac, D. Helmberger, E. Hauksson, R. Chu, M. Simon, T. Herring, and R. Briggs (2011). Superficial simplicity of the 2010 El Mayor–Cucapah earthquake of Baja California in Mexico, *Nature Geosci.* **4,** 615–618.

Wilcox, R. E., T. P. Harding, and D. R. Seely (1973). Basic wrench tectonics, *Am. Assoc. Pet. Geol. Bull.* **57,** no. 1, 74–96.

Wolfe, F. D., J. H. Shaw, A. Plesch, D. J. Ponti, J. F. Dolan, and M. R. Legg (2019). The Wilmington blind-thrust fault: An active concealed earthquake source beneath Los Angeles, California, *Bull. Seismol. Soc. Am.* **109,** no. 5, 1890–1906.

Woodring, W. P., M. N. Bramlette, and W. S. W. Kew (1946). Geology and paleontology of Palos Verdes Hills, California, *U.S. Geol. Soc. Profess. Pap. 207*, 145 pp.

Wright, T. L. (1991). Structural geology and tectonic evolution of the Los Angeles Basin, California, in *Active Margin Basins*, K. T. Biddle (Editor), American Association of Petroleum Geologists, Tulsa, Oklahoma, 35–79.

Yang, W., and E. Hauksson (2013). The tectonic crustal stress field and style of faulting along the Pacific North America Plate boundary in Southern California, *Geophys. J. Int.* **194,** no. 1, 100–117.

Yang, W., E. Hauksson, and P. M. Shearer (2012). Computing a large refined catalog of focal mechanisms for Southern California (1981–2010): Temporal stability of the style of faulting, *Bull. Seismol. Soc. Am.* **102,** no. 3, 1179–1194.

Yeats, R. S., and J. M. Beall (1991). Stratigraphic controls of oil fields in the Los Angeles Basin a guide to migration history: Chapter 7, in *Active Margin Basins*, K. T. Biddle (Editor), AAPG Special Volumes, Tulsa, Oklahoma, 221–235.

Yerkes, R. F., D. S. Gorsline, and G. A. Rusnak (1967). Origin of Redondo Submarine Canyon, Southern California, *U.S. Geol. Surv. Res. 1967*, C97–C105.

Yerkes, R. F., T. H. McCulloh, J. E. Schoellhamer, and J. G. Vedder (1965). Geology of the Los Angeles Basin, California: An Introduction, *U.S. Geol. Surv. Profess. Pap. 420-A57*, doi: 10.3133/pp420A.

Ziony, J. I. (1985). Evaluating earthquake hazards in the Los Angeles region; An earth-science perspective, *U.S. Geol. Surf. Profess. Pap. 1360*, US Government Printing Office, 505 pp.

Manuscript received 19 October 2021
Published online 14 July 2022